Photonic Integrated Circuit Architecture for Radio-over-Fibre Applications

by

Mehedi Hasan

A Thesis submitted to the Faculty of Graduate and Postdoctoral Studies

in partial fulfillment of the requirements for the degree of

MASTER OF APPLIED SCIENCE

in Electrical and Computer Engineering

Ottawa-Carleton Institute of Electrical and Computer Engineering

University of Ottawa

Ottawa, Canada

May, 2015

Abstract

The aim of the research presented in this thesis is to develop photonic integrated circuit (PIC) for Radio-over-Fiber (RoF) application. As such, at the beginning of the thesis, a dual-function photonic integrated circuit for microwave photonic applications is proposed. The photonic circuit is arranged to have two separate output ports, and depending upon the RF input signal strength, it provides either tunable millimeter wave carriers by frequency octo-tupling of the RF signal or frequency up-conversion of a microwave signal from the electrical to the optical domain. The circuit exploits the intrinsic relative phases between the ports of multi-mode interference couplers (MMI) to provide all the static optical phases needed, hence drift free. In the middle of thesis, a generalized architecture having N parallel phase modulators driven electrically with a progressive $2\pi/N$ phase shift is analyzed. The proposed design is justified by computer simulation for N=8 architecture with properly determined optical phase shifts to generate frequency multiplication of an electrical signal. The front- and back-end of the circuit comprises 4×4 MMI couplers enclosing an array of four pairs of phase modulators and 2×2 MMI couplers. The proposed design for frequency multiplication requires no optical or electrical filters; the operation is not limited to carefully adjusted modulation indexes. Later on, a generalized approach for achieving frequency multiplication using two cascades MZM is presented. The proposed design consists of a Mach-Zehnder interferometer with each arm containing a pair of Mach-Zehnder modulators (MZM) in series as a means of optoelectronic frequency multiplication (octo-tupling and quattourviginti-tupling). The circuit requires no electrical or optical filters. There is no requirement to carefully adjust the modulation index to achieve correct operation of the octo-tupler. A comparison is made with an alternative functionally equivalent single-stage parallel MZM circuit discussed herein the thesis. Finally, the thesis describes the generation of the same magnitude but opposite sign high order single optical side band from its output ports by using a RF source. A single stage parallel Mach-Zehnder Modulator (MZM) and a two-stage series parallel MZM architecture is described and their relative merits and demerits discussed. As an illustration of a prospective application it is shown how the circuit may be used to transport radio signals over fibre for wireless access; generating remotely a mm-wave carrier modulated by digital IQ data. A detail calculation of symbol error rate is presented to

characterise the system performance. A mathematical analysis is provided to describe the principle of operation for all the proposed design and validated by commercially available industrial standard simulation tool.

Dedication: I would like to dedicate this thesis to my supervisor Professor Trevor James Hall and my beloved wife Mansura Jasmine.

Acknowledgement

My heart-felt thanks and greetings to my supervisor, Professor Trevor James Hall, without his continuous support and guidance this thesis would not have been possible. He is very generous and diligence. His encouragement and quick response to any problems I have faced; have been a great motivation for me to continue this valuable work. I must have to mention one thing that, whenever I sent him an email at late night, I got reply right away; furthermore, he replied my queries continuously in the weekends by sacrificing his leisure time. All of his enthusiasm inspired me to work hard for the thesis to make him happy. Thanks are also due to Dr. Sawsan Abdul-Majid and Dr. Ramon Maldonado-Basilio, Photonic Technology Laboratory (PTL) University of Ottawa, for their kind assistance over the past two years, especially at the beginning when I was struggling hard to coop with new environments . I also would like to express my gratitude to all the members of PTL for their contribution to a friendly working environment. My deepest gratitude to my wife for scarifying her career for my study and took the responsibility to run the family, so that I can give my best. Special thanks to my closest Mahfuzul Haque for his mental support and arranging the necessary financial support to accomplish all the formalities before my departure. Thanks to Canadian government for issuing my visa. Finally I give a special thank you to my parents who sacrificed a lot for me throughout my life. I am indebted to all my relatives and friends for their continuous support, closely or remotely, during my study.

Table of Contents

List of Figures

List of Tables

List of Abbreviations

MMI	Multi-Mode Interference Coupler
MZI	Mach-Zehnder Interferometer
MZM	Mach-Zehnder Modulator
PIC	Photonic Integrated Circuit
SSB	Single side-band
GMZI	Generalised Mach-Zehnder Interferometer
MATP	Maximum transmission point
MITP	Minimum transmission point
SHSR	Side harmonic suppression ratio
RoF	Radio-over-Fibre
DFB	Distributed Feedback
CW	Continuous Wave
PM	Phase Modulator
PD	Photo-diode
LD	Laser-diode
RF	Radio Frequency
DC	Direct Current
AWG	Arrayed Waveguide Grating
IL	Interleaver
WLAN	Wireless Local Area Network
MIMO	Multiple Input Multiple Output
LTE	Long -Term Evolution
DAS	Distributed Antenna System
RAU	Remote Antenna Unit
GHG	Greenhouse Gas
IM	Intensity Modulation
DD	Direct Detection
QPSK	Quadrature phase shift keying
QAM	Quadrature Amplitude Modulation
PRBS	Pseudorandom Binary Sequence
LSB	Lower side-band

USB	Upper side-band
SER	Symbol Error Rate
EVM	Error Vector Magnitude

Chapter 1. Introduction

This chapter describes the background and motivation of the thesis. It also defines the objectives of this research work and how the thesis is structured to meet the goal.

1.1 Background and Motivation

In the last two decades, wireless communication has experienced enormous growth. Not more than 0.2% (11 million) of the world's population (5 billion) had access to a mobile phone in 1991 [1], which is 2% of fixed line telephone subscribers, whereas, in May, 2014, the number of mobile phone users was more than 7 billion of the total population, 96% [2]. The most important turning point in the history of mobile telephony happened when the number of fixed-line subscribers were overtaken by mobile subscribers in 2002 [3]. Wireless Local Area Networks (WLANs), first introduced in 1997 to provide services in public places such as airport terminals, parks, etc., have also had noticeable growth, due to their distinctive features like narrow band services, offering a data transmission rate of up to 54 Mbps with carrier frequencies in the range of 2.4 GHz (IEEE 802.11a/g) and 5 GHz (HiperLAN/2) in the license-free ISM (industrial, scientific and medical) radio bands. The rapid proliferation of WLAN, brings it to home services (private) with a cable access modem, through digital subscriber lines, and hence provides a high data rate to fixed wireless subscribers. Tremendous Internet growth due to technological advancement and competition among mobile operators and the consequent demand for high speed applications like voice and video has brought about the concept of ubiquitous connectivity (communication anytime, anywhere, and with anything). As such wireless local networks must provide its subscribers high transmission capacity with sufficient coverage area. Furthermore, the mobility offered by mobile systems is much better than WLANs. With current fibre penetration, high speed 100 Mbps Ethernet is now at the doorstep of the end user (because of Fibre at Home/Curb/X, FTTH/C/X). The eagerness of the subscriber having the same or more demand in terms of transmission capacity on wireless puts enormous pressure on the broadband wireless system. As such, taking into account the capacity of transmissions, coverage is also a major issue. From the Shannon channel capacity theorem, low carrier frequencies offer low bandwidth. This is part of the reason that narrowband wireless access systems offer small capacity as they operate at lower frequencies, such as the operating frequencies of GSM which are 900

MHz or 1800 MHz with a 200 KHz channel spectrum including 20 KHz for a guard band, and UMTS which has a 4 MHz bandwidth with operating frequencies around 2 GHz [5]. As such, in LTE technology the channel bandwidth is flexible up to 20 MHz with some scaling factors and multiple input and multiple output (MIMO) reception, while the operating frequencies are up to 2.6 GHz maximum (Rogers, Bell Canada). The LTE-Advanced technology offers a higher bit-rate than LTE because of scalable system bandwidth up to 100 MHz exceeding 20 MHz [6].

The transmission capacity can be increased by transmitting at higher frequencies at around 60 GHz, the unlicensed millimetre wave (mm-wave) frequencies (57-64 GHz). The problem is, at high frequencies the transmission path loss is high which leads to a reduced service area (cell). At high frequencies, high frequency transistors and power amplifiers are very costly and they are also power hungry. The low-frequency operating system has the advantage of low power consumption. The radical climatic behaviour has drawn the urgent attention of society to reduce the emissions of greenhouse gas (GHG), and has brought the concept of a GREEN ICT with low power consumption and reduced CO_2 emissions. On top of that, a smaller cell implies more RAUs (Remote Antenna Units) to cover the whole serviced area to meet the demand of the people, which will lead to many complexities of the network, like cost, installation, and maintenance, so, there must be a trade-off between capacity and coverage. This bottleneck has brought a new paradigm of broadband wireless access networks. In this situation, the radio-over-fibre (RoF) paradigm with a distributed antenna system (DAS) came into play with enormous opportunity. The energy consumption in optical networks is as low as a few orders of magnitude, in comparison to other technologies. With lower energy consumption, Radio-over-Fibre is one of the possible solutions for broadband wireless access with high capacity and coverage.

For multiple purposes radio transmission over fibre is used, especially for Cable Television (CATV) networks and base stations used for satellite communications. The term RoF (Radio over Fibre) is usually applied when it is used to facilitate wireless access. The simplest method for transporting radio over fibre (RoF) refers to an analog transmission where RF signals directly modulate the intensity of the light source, and are then transmitted through an optical fibre for wireless access. At the receiver direct detection is used in the photo detector

to recover the RF signal. This method is called IM/DD and this is the simplest method for a Radio over Fibre link.

The Photonic Technology Laboratory are investigating, inter alia, wireless access networks capable of delivering the ubiquitous broadband and computing access envisaged in the sustainable city of the third millennium [7]. In a radical departure from the traditional radio-over-fibre paradigm, the architectures of interest feature digital coherent optical transport (see Figure 1.1). The weakest link in this architecture has been identified as the single side-band modulator or up-conversion mixer at the front end of the uplink (Figure 1.1(b)). The implementation of the up-conversion mixer acquires even greater relevance in coherent optical RoF systems, when the transport of m-ary quadrature amplitude modulation (mQAM) provides technical and environmental advantages relative to the traditional analog RoF systems [7].

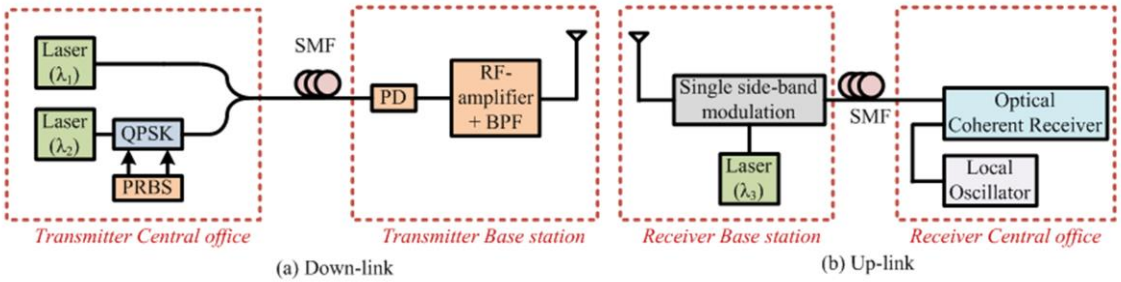

Fig. 1.1. Adopted architecture. Down-link (a) and Up-link (b). PRBS: Pseudo-Random Binary Sequence; QPSK: Quadrature Phase Shift Keying; SMF: Single-Mode Fibre, PD: Photo-Detector. RF: Radio-Frequency. BPF: Band-Pass Filter.

1.1.1 Frequency Up-Conversion or Single Side-band Modulation

The coherent RoF system described requires frequency up-conversion (mm-wave to optical) or single side-band (SSB) modulation in the uplink. In coherent systems, it is a fundamental requirement to be able to change the frequency of a signal while preserving its phase and amplitude information. To the best of the author's knowledge, an integrated light SSB modulator based on a Ti diffused $LiNbO_3$ optical waveguide was reported for the first time in 1981 [8]. The circuit configuration is same as the dual-parallel Mach-Zhender modulator (DP-MZM) driven by an in-phase and quadrature signal at 2 GHz

which is well below the mm-wave frequency. Since then, there has been a plethora of publications [9-22] describing different techniques of achieving frequency up-conversion. Among them, the operation is achieved in [9-11] by using mm-wave, where a custom electro-absorption modulator (EAM) is used to amplitude-modulate a distributed feedback laser (DFB) externally. Optical filter (for example, fibre-Bragg grating (FBG)) is then used to extract a single side-band. The conversion efficiency is low, which reduces sensitivity of the up-link. Moreover, the EAM, DFB laser, and FBG must be very closely matched in frequency of operation, which will entail energy hungry temperature control. On the other hand, electro-optic mixers use electro-optic materials to phase-modulate optical carriers. Typically, several modulators are combined to form Mach-Zehnder modulators (MZM) that amplitude-modulate the in-phase (I) and quadrature (Q) components of the optical carrier. The I and Q components are derived using precise optical phase-shifters. Combined with precise electronic phase shifts or adjusting the amplitude of the drive signal, these arrangements can suppress the carrier and one sideband, resulting in the desired phase and amplitude information preserving frequency translation (up-conversion). The implementation of SSB on architectures utilizing single MZM [12-14], multiple MZM [15] and using DP-MZM [16] have been intensively investigated. To minimize trimming, it is advantageous in integrated circuits to exploit phase shifts that are intrinsic to the topology (and hence are broadband and temperature insensitive) of the optical and electrical waveguides (e.g. the phase shift $\pi/2$ between the arms of a 3dB coupler and more generally the phase-relations due to self-imaging in MMIs [17-18]). The use of the intrinsic phase relationship between ports of a MMI coupler has been recently proposed to enable I and Q modulation [19] or to improve the linearity of an electro-optic modulator by selective suppression of unwanted inter-modulation products [20-22]. In [19] additional phase-shift elements must be added to two arms of the structure. These may be implemented using a statically biased electro-optic or a thermo-optic phase shift element which reintroduces the need for trimming and drift compensation. In [20-21] the architectures rely on the phase relationship between ports of an MMI coupler used as a splitter. After phase modulation, the beams are recombined using a ‘combiner’ element with equal optical path lengths between its output and all its input ports. The architecture is verified by VPIcomponentMakerTM simulation software

using supplied component models including a ‘combiner.’ If an experimental test had been performed, the authors would have discovered that the required ‘combiner’ is nonphysical. Any ‘combiner’ is a splitter used in reverse and in general will have different phase relationships between its ports. Hence these architectures also require the addition of static phase shift elements. As such [21-22], improved performance is achieved as DP-MZM offers selective suppression (Other than +1 and -3, all other harmonics are suppressed, in principle at least) of unwanted harmonics over dual drive (DD) MZM [16]. The implementation of SSB using DP-MZM, requires the upper and lower sub-MZM operating at a minimum transmission point (MITP), which requires DC bias. The need of DC bias in MZMs results in drift that has been acknowledged as a serious issue and has led to a substantial volume of literature on the physical mechanisms responsible [23-24] and its alleviation by sophisticated stabilisation mechanisms [25-28].

1.1.2 Generation of mm-wave

The fundamental operational principle at the heart of microwave photonics is the heterodyne beating of two optical carriers separated in frequency at a high speed photo-detector, which offers a conceptually simple means of generating a widely-tunable microwave carrier. To ensure the generation of a spectrally pure microwave carrier, the two optical carriers must be correlated in phase. Although there are various ways by which correlated optical carriers may be generated, external modulation of a laser is particularly attractive because it offers high-stability tunable spectrally-pure microwave carriers with system simplicity. The basic principle is to phase-modulate an optical carrier by a radio frequency (RF) electrical carrier via a suitable electro-optic modulator. The modulation results in an optical spectrum containing a multitude of phase-correlated lines separated by the RF frequency.

Numerous circuit architectures have been conceived [29-47] that contain several phase modulators driven from the same optical and electrical sources but with carefully chosen relative phase-shifts combined in a network such that only two optical lines separated by a desired multiple of the RF frequency have significant amplitude at the output port. The majority of the circuits proposed [29-42] employ essentially a single stage generalized Mach-Zehnder Interferometer (GMZI) architecture in which N phase modulators are interconnected

by a 1:N splitter and N:1 coupler. When N is even, the individual phase modulators may be paired and the basic element may be considered to be a dual-drive or most often differential-drive Mach-Zehnder Modulator (MZM). One of the first experimental demonstrations of a frequency doubler based on the remote heterodyne concept was reported over 20 years ago using a single laser source together with a LiNbO3 Mach-Zehnder modulator (MZM) to obtain a narrow line-width 36 GHz electric signal with a peak power around -50 dBm and signal-to-noise ratio (SNR) of over 40 dB [29]. Thereafter, different higher order multiplication factors have theoretically and experimentally been reported, achieving frequency quadrupling [29-32], sextupling [33-34], octo-tupling [35-38] and beyond [39-41]. Regarding frequency quadrupling, for instance, a MZM biased at the maximum transmission point to suppress the odd order side-bands is used in addition with an optical notch filter to generate a 32-50 GHz mm-wave [30] or using an optical filter to generate mm-waves up to 64 GHz [31]. An integrated design comprising two MZMs the full-bias point and placed in the arms of an outer MZM biased at the null point is proposed as an optical filter-less approach to obtain second order sidebands with an optical and harmonic distortion suppression ratio of more than 36 dB, generating a -30 dBm mm-wave carrier at 40 and 72 GHz [32]. Configurations based on DP-MZM are proposed for frequency sextupling, where the two sub-MZMs are biased at the minimum transmission point and the outer MZM is biased at the maximum transmission point [33]. Designs based on a polarization modulator and wavelength-fixed optical notch filter [34] have been proposed as frequency sextupling approaches to generate tunable carriers from 66 to 114 GHz. Similar designs based on nested MZMs [35] with RF drive adjustment, dual-parallel MZMs (DP-MZM) in combination with notch filters [36], four-parallel phase modulators [37] or two parallel DP-MZM [38] with Y-splitter and combiner at the front and back end have been experimentally and theoretically studied for frequency octo-tupling. Higher frequency multiplication factors have been investigated. For instance, second order harmonics out of a dual-parallel MZM are used to implement degenerate four-wave mixing in a semiconductor optical amplifier to achieve frequency 12-tupling [39]. Two-electrode dual-parallel MZMs with carefully adjusted radio frequency drive signals have also been studied and demonstrated by numerical simulations for 12-tupling frequency multiplication [40]. A configuration of three MZMs in parallel has

been proposed for frequency 6-tupling, 12-tupling, and 18-tupling depending upon the bias conditions on the modulators [41].

On the other hand, a lesser number of proposals have considered two-stage architectures in which the basic element, i.e., MZMs, are connected in series [42-46] or both in series and parallel [47].Circuit designs for frequency multiplication by quadrupling, sextupling and octo-tupling using a two-stage cascade MZM structure are proposed in references [42-46]. The MZM modulators are biased at the minimum transmission point (MITP) with the RF drive having 90° phase difference between stages to obtain the frequency quadrupling function [42]. A similar multiplication factor is obtained by driving both the MZM with same RF drive but inserting a tunable optical delay line to adjust the relative phase of the sidebands generated by the first stage [43]. By setting the first MZM at the MITP and the second MZM at the maximum transmission point (MATP) or vice-versa, frequency sextupling is achieved [44, 46]. By biasing both the MZM at the MATP frequency, octo-tupling is achieved with appropriate adjustment of the tunable optical delay line and RF drive level [45-46]. The use of discrete components, the need for static DC bias points, and the use of carefully adjusted electrical drive levels or optical filtering to suppress a particular unwanted harmonic are among the most common demerits of these designs. A summary of the works mentioned in the preceding is given in Table 1.1.

Table 1.1 Summary of the previous work related to frequency multiplication.

Reference	**Function**	×	**Exp/Sim**	**Comment**
O'Reilly 1991[29]	Frequency multiplier	2	Exp	MZM is biased at MITP to suppress all the even order harmonics.
Qi 2005 [30]	Frequency multiplier	4	Exp	FBG used to suppress carrier
Yu 2007 [31]	Frequency multiplier	4	Exp	MZM biased at MATP, Optical interleaver is used to suppress the carrier.
Lin 2008 [32]	Frequency multiplier	4	Exp	DPMZM Outer MZI biased at MITP

Shih 2010 [33]	Frequency multiplier	6	Sim	DPMZM Orders 2,4,5,6 are suppressed. Order 1 is suppressed by adjustment of the RF drive level leaving ± 3 orders significant strength.
S Pan 2010 [34]	Frequency multiplier	6	Exp	Polarization modulator Notch filter is used to suppress unwanted harmonics.
Zhang 2012 [35]	Frequency multiplier	8	Exp	Orders 1, 2, 3 are suppressed. Order 0 is suppressed by FBG. Leaving ± 4 orders significant in strength.
Ma 2008 [36]	Frequency multiplier	8	Sim	DPMZM RF drive level adjusted to suppress carrier
Guemri 2014 [37]	Frequency multiplier	8	Sim	Orders 1, 2, 3 are suppressed. Order 0 is suppressed by adjustment of the RF drive level.
Yin 2011[38]	Frequency Multiplier	8, 16	Sim	2 parallel DPMZM between y-splitter / combiners. RF drive level is adjusted to suppress carrier and other unwanted harmonics.
Shih 2010 [39]	Frequency multiplier	12	Sim	DPMZM is used with four wave mixing technique. Optical interleaver is used to suppress unwanted harmonics
Z. Zhu 2013 [40]	Frequency multiplier	12	Sim	Orders 0, 1, 3, are suppressed. Order 2 is suppressed by adjustment of the RF drive. Leaving ± 6 orders significant

				in strength
Chen 2011 [41]	Frequency multiplier	6, 18	Sim	Unsuppressed orders are -9, -3, 3, 9. Order 3 suppressed by adjustment of RF drive level to achieve × 18
Zhang 2007 [42]	Frequency Multiplier	4	Exp	2 MZM in series. MZMs biased at (MITP, MITP)
Chi 2008 [43]	Frequency Multiplier	4	Exp	2 MZM in series. MZMs biased at (MITP, MITP); tuneable optical delay between stages
Mohammed 2008 [44]	Frequency Multiplier	6	Exp	2 MZM in series. MZM biased (MITP,MATP) or (MATP, MITP); RF drive level adjusted to suppress unwanted orders
Li 2010 [45]	Frequency Multiplier	8	Exp	2 MZM in series. Tunable optical delay is used. RF drive level adjusted to suppress unwanted orders
Li 2010[46]	Frequency Multiplier	4, 6, 8	Exp	2 MZM in series. FBG is used & tunable optical delay are used to suppress unwanted orders.
Gao 2014 [47]	Frequency Multiplier	6	Exp	Intensity modulator in series with DPMZM. Controlled DC bias is used to suppress the unwanted harmonics

1.1.3 High order USB and LSB Separation for Remote Heterodyning

A significant number of architectures based on external modulation have been proposed [29-47] to achieve different order frequency multiplication. A common feature of all the reported circuit designs is that the pair of high-order harmonics separated by the desired RF carrier frequency (± 4 for frequency octo-tupling) is emitted from the same output port. The pair of carriers must therefore be separated as the data to be transported must modulate only one of them. This can be done by using frequency selective components such as arrayed waveguide gratings (AWGs) or an optical interleaver (IL), but this severely restricts the tuning range to the bandwidth of the frequency selective components and introduces frequency alignment issues that require temperature stabilization. Because of this, there is a requirement for a circuit that can generate two high order harmonics that are emitted from different output ports (for example, $+4$ from one port and -4 from another port). This carrier separation eliminates the need for thermal stabilization.

1.2 Aim and Objectives

The main aim of this thesis is to design a frequency up-conversion mixer for a coherent RoF application that can overcome the previously reported shortcomings such as the stability, conversion efficiency and, of course, the footprint of the chip. Later on, the thesis focuses on the generation of a microwave frequency multiplication circuit that overcomes the previous shortcomings such as using a filter or adjusting the RF drive to achieve a particular function. This investigation includes generalised Mach-Zhender Interferometer (GMZI) architecture in which N phase modulators are interconnected by a 1:N splitter and N:1 coupler. When N is even, the individual phase modulators may be paired and the basic element may be considered to be a dual-drive or most often differential-drive Mach-Zehnder Modulator (MZM). The thesis also investigates the two-stage cascade architecture for microwave frequency generation. Finally, the generation of high order LSB and USB separation for remote heterodyne in RoF applications are also investigated.

The specific objectives are:

1) to improve the performance (e.g., conversion efficiency, linearity and dynamic range, power consumption, footprint, and stability) of such electro-optic up-conversion mixers.

2) to find a new design which can overcome the previous shortcomings for microwave frequency multiplication. The goal is to analysis a wide range of circuit architecture such as parallel structure, and series-parallel architecture.

3) to design a new circuit that can generate high-order LSB and USB from different output ports to use in remote heterodyning for RoF application.

1.3 Structure of the Thesis

The thesis has been structured into six (6) chapters to demonstrate the achievements in research to meet the objectives mentioned above.

Chapter 1 describes the motivation and the background of the research. It addresses the previous work done in the topics and their bottleneck. This chapter also summarizes the objectives of the thesis and achievements during the period of research.

Chapter 2 introduces a dual-function photonic integrated circuit for microwave photonic applications. The circuit consists of four linear electro-optic phase modulators connected optically in parallel within a generalized Mach-Zehnder interferometer architecture. The photonic circuit is arranged to have two separate output ports, and depending upon the RF input signal strength, it provides either tunable millimeter wave carriers by frequency octo-tupling of the RF signal or frequency up-conversion of a microwave signal from the electrical to the optical domain. The operation of the proposed dual-function photonic integrated circuit is verified by computer simulations. Practical inaccuracies such as power imbalance and phase errors between the ports of MMIs and length of the waveguide connected between the RF source and phase modulators are taken into account and analyzed.

In Chapter 3, a generalized architecture having N parallel phase modulators driven electrically with a progressive $2\pi/N$ phase shift is analyzed. Based on the proposed architecture, a theoretical approach is presented. The proposed architecture is justified by computer simulation for N=8 architecture with properly determined optical phase shifts to generate frequency multiplication of an electrical signal. Furthermore, using the intrinsic phase relationship among the ports of 4×4 MMI, a functionally equivalent circuit of the

N=8 architecture is proposed, which overcomes the requirements of static optical phase shift in N=8 architecture. Ideal and imperfect power imbalances in the multi-mode interference couplers, as well as ideal and imperfect phases of the electric drives to the phase modulators are analyzed.

Chapter 4 summaries the generalized approach for achieving frequency multiplication using a cascade of two MZMs. It includes the theoretical analysis and operating conditions of achieving different frequency multiplication factors. Later on, using the concept of general theory, a more robust and superior frequency multiplication architecture is demonstrated. A transfer matrix representation is used to describe the operation of the architecture. The theoretical predictions are validated by simulations performed using a commercially available software tool. The simulations also allow an assessment of the impact on the circuit operation of deviations from the ideal of its components such as the finite extinction ratio of the MZMs, power imbalances and phase error at the input coupler and phase error of the applied RF signals. Finally, a comparison is made with an alternative functionally equivalent single-stage parallel MZM circuit discussed in the previous chapter.

Chapter 5 demonstrates the generation of the same magnitude but opposite sign high-order single optical sideband from its output ports using an RF source. The theoretical analysis is validated by computer simulation. As an illustration of a prospective application it is shown how the circuit may be used to transport radio signals over fibre for wireless access, remotely generating an mm-wave carrier, modulated by digital IQ data. A detailed calculation of symbol error rate is presented to characterise the system performance.

Chapter 6 summarises the findings in the thesis, makes conclusions and offers recommendations for further work.

VPIcomponentMaker^{TM} (version 9.1) simulation software is used to simulate the all the considerations throughout the thesis.

1.4 Original Contributions and Achievements

The thesis contributes to the advancement of the field of RoF technology and microwave photonics.

The contributions of the author include:

1. A photonic integrated circuit for frequency up-conversion is presented. The circuit consists of four linear electro-optic phase modulators connected optically in parallel within a generalized Mach–Zehnder interferometer architecture. The operation of the circuit does not require any DC bias; hence no complex circuit is required to control the drift as there is no drift. It is also shown how a minor modification in the design enables the reuse of much of the circuit to obtain a distinct application. The proposed design also demonstrates how the phase relationship between the ports of the 2×2 MMI (2×1 combiner or 1×2 splitter) can be used to form an MZM without any DC bias.
2. A DC bias-less, filter-less novel frequency octo-tupler is presented. Moreover, the operation of the circuit is not restricted by careful adjustment of the modulation index. The proposed design shows how the phase relationship among the output ports of the 4×4 MMI can be used at the front and back end with careful selection of the phases of applied RF signal to the phase modulators to obtain a particular operation, i.e., an octo-tupler. A theoretical analysis is also developed to show that "any unwanted harmonics can be suppressed while the harmonics of interest can be maximized by careful selection of the static optical phase and phases of the RF signal."
3. A frequency octo-tupler circuit based on two-stage architecture is also presented as an improvement of the current knowledge and a comparison between parallel architecture and a two-stage series-parallel circuit is presented.
4. A novel photonic integrated circuit is proposed in this thesis, that can generate high order harmonics (same but opposite) from the two output ports ($+2^{nd}$ from the upper ports and -2^{nd} from the lower ports). This design overcomes the requirement of AWG or optical IL as it separates the harmonics by design.

The results demonstrated in this thesis were obtained during a period of study at the University of Ottawa to fulfill the requirement of getting an M.A.Sc. The work was carried out under the supervision of Professor Trevor James Hall from fall 2013 to summer 2015 at

the Photonic Technology Lab (PTL). The following publications related to this research work (thesis) were published or submitted for publication during this period.

[1]**M. Hasan**, R. Maldonado-Basilio, and T. J. Hall, "Dual-function photonic integrated circuit for electro optic frequency multiplication or single-side-band modulation," Optics Letters, **40** (11), 2501 (2015).

[2]**M. Hasan**, R. Maldonado-Basilio, **T. J. Hall**, "Comments on X. Yin, A. Wen, Y. Chen, and T. Wang, 'studies in an optical millimeter-wave generation scheme via two parallel dual-parallel Mach-Zehnder modulators", Journal of Modern Optics, **62**(7), pp. 581-583 (2015).

[3]**M. Hasan**, R. Gumeri, R. Maldonado-Basilio, F. Lucarz, J-L de Bougrenet and **T. J. Hall**, "Photonic integrated circuit for frequency 8- and 24-tupled millimeter wave signal generation," Optics Letters, **39**(24), pp. 6950-6953 (2014).

[4]R. Maldonado-Basilio, **M. Hasan**, H. Nikkah, S. Abdul-Majid, R. Gumeri, F. Lucarz, J-L. de Bougrenet and **T. J. Hall**, "Electro-optic up-conversion mixer amenable to photonic integration," Journal of Modern Optics, 2015 (Online).

[5]**M. Hasan**, R. Maldonado-Basilio, **T. J. Hall**, "An efficient microwave photonic frequency octo-tupler with high spurious sideband suppression," Optics Communication (Accepted) August, 2015.

[6]R. Maldonado-Basilio, **M. Hasan**, R. Gumeri, F. Lucarz, **T. J. Hall**, "Generalized Mach-Zehnder interferometer architectures for radio frequency translation and multiplication: suppression of unwanted harmonics by design," Optics communication (online) May, 2015.

[7]**M. Hasan**, and **T. J. Hall**, "A PIC for high order USB and LSB separation for remote heterodyning," (Submitted) June, 2015.

Chapter 2. Frequency up-conversion or frequency octo-tupling

2.1 Introduction

In the past two decades or so there has been a plethora of publications [8-16, 29-42] in the field of microwave photonics that have described essentially the same generalized Mach-Zehnder Interferometer (MZI) circuit architecture: a $1 \times N$ splitter directly interconnected to a $N \times 1$ combiner via an array of N electro-optic $LiNbO_3$-based phase modulators, each adapted to particular design goals. The applications have generally been to single-side-band (SSB) modulation [8-16, 20-22] or electro-optic microwave signal frequency multiplication [29-42]. The difference between the circuits proposed have largely concerned variations of the static optical and electrical phase shifts required or the implementation of an equivalent circuit using standard Mach-Zehner modulators (MZM) rather than individual phase-modulators (PM) as the basic building brick. The aim of this chapter is to show how to use the intrinsic phase relations between the ports of splitters and combiners and specifically multi-mode interference (MMI) couplers to implement the static optical phase shifts required by these circuits, thereby avoiding the need to apply static DC bias to the electro-optic modulators and the associated drift issues that otherwise require complex stabilization circuitry [25-27]. As the best of authors knowledge, for the first time a DC bias-less frequency up-converter is reported. It is also shown that, relatively minor modifications or additions to a particular circuit in the generalized MZM class [48] may enable the reuse of much of the circuit for distinct applications, heralding the prospect of a first general purpose microwave photonic integrated circuits. While $LiNbO_3$ technology offers a mature solution to the small scale integration of MZM structures, this work anticipates photonic integrated circuits based on Si and/or InP material integration platforms emerging as the preferred choice [49]. In this context the continuous advances made in improved speed, linearity, footprint, and energy consumption of electro-optic phase modulator devices in both material platforms [50-53] augurs well. Some of the recent demonstration of Silicon-organic hybrid (SOH) IQ modulator for transmitting 16 QAM at 112 Gbit/s [50]; InAlGaAs-based electro-optic modulators with low drive voltage ($v_\pi = 0.77V$) and an exceeding bandwidth of 67

GHz [51]; athermal InP based twin IQ modulators having footprints of 1.2 mm × 13 mm for 56 Gb/s QPSK [52]; anticipates that modulator with improved performance is forthcoming.

2.2 Principle of operation

Fig 2.1 provides a schematic diagram of a circuit capable of the dual function of either millimeter wave generation by frequency octo-tupling a microwave RF input signal or frequency up-conversion to the optical domain of an RF input signal in the electronic domain by carrier suppressed SSB modulation. The latter being equivalent to the modulation of an optical carrier by baseband in-phase and quadrature (I&Q) signals. As illustrated in the schematic diagram, the 1×2 symmetric splitter together with the 2×1 symmetric combiner form an outer MZI with two arms. Each arm itself contains an inner MZM sub-circuit formed by a 2×2 MMI splitter (with one input port unused) interconnected with a 2×2 MMI combiner, and linear electro-optic phase modulators in each arm that are differentially driven. The outer MZI is arranged to have two separate output ports, namely E_1&E_2, and D. In one output, the two opposing ports (d_2) to the two input ports (a_1) are combined in a symmetric 2×1 MMI and provide the frequency octo-tupling of the RF input signal after a square-law photo-detector. On the other hand, the two remaining ports (d_1) are combined in a 2×2 MMI and provide the upper (E_1) and lower (E_2) SSB modulation.

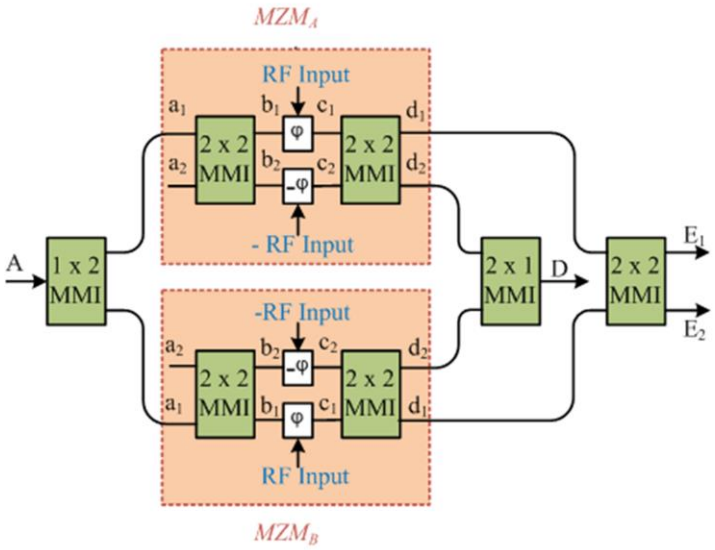

Fig. 2.1. Schematic diagram of the proposed dual-function photonic integrated circuit.

The transmission of each inner MZM for an input a_1 and an unused input port a_2 can be written as:

The input vector $[a_1 \quad a_2]$ is related to the output vector $[d_1 \quad d_2]$ through:

$$\begin{bmatrix} d_1 \\ d_2 \end{bmatrix} = \frac{1}{2}\begin{bmatrix} 1 & -i \\ -i & 1 \end{bmatrix}\begin{bmatrix} e^{i\varphi} & 0 \\ 0 & e^{-i\varphi} \end{bmatrix}\begin{bmatrix} 1 & -i \\ -i & 1 \end{bmatrix}\begin{bmatrix} a_1 \\ a_2 \end{bmatrix} \tag{2.1}$$

$$= i\begin{bmatrix} sin(\varphi) & -cos(\varphi) \\ -cos(\varphi) & -sin(\varphi) \end{bmatrix}\begin{bmatrix} a_1 \\ a_2 \end{bmatrix} \tag{2.2}$$

where:

$$\begin{bmatrix} d_1 \\ d_2 \end{bmatrix} = \frac{1}{\sqrt{2}}\begin{bmatrix} 1 & -i \\ -i & 1 \end{bmatrix}\begin{bmatrix} c_1 \\ c_2 \end{bmatrix} \tag{2.3}$$

and

$$\begin{bmatrix} c_1 \\ c_2 \end{bmatrix} = \begin{bmatrix} e^{i\varphi} & 0 \\ 0 & e^{-i\varphi} \end{bmatrix}\begin{bmatrix} b_1 \\ b_2 \end{bmatrix} \tag{2.4}$$

are the transfer functions of the 2×2 MMIs and the array of optical phase modulators, respectively. In addition, $\varphi = \pi\, v/v_\pi$ is the optical phase shift impressed by the phase modulator with switching voltage of v_π by the application of a differential signal with amplitude v. From Eq. (2.2), it can be seen that this MZM architecture acts as a cross-over for $\varphi = 0$ and hence the MZM is biased at the minimum transmission point for an output taken from opposing ports. For the target application, ports a_2 and d_2 are unused. Hence,

$$d_1 = isin(\varphi)a_1 \tag{2.5}$$

$$d_2 = -icos(\varphi)a_2 \tag{2.6}$$

2.2.1 SSB Modulation

Using the transfer function (2.5) for $MZM_{A,B}$, the output of the optical up-conversion mixer can be represented by:

$$\begin{bmatrix} E_1 \\ E_2 \end{bmatrix} = i\frac{1}{2}\begin{bmatrix} 1 & -i \\ -i & 1 \end{bmatrix}\begin{bmatrix} sin(\varphi_a) & 0 \\ 0 & sin(\varphi_b) \end{bmatrix}\begin{bmatrix} 1 \\ 1 \end{bmatrix}[A] \tag{2.7}$$

$$= \frac{1}{2}\begin{bmatrix} isin(\varphi_a) + sin(\varphi_b) \\ sin(\varphi_a) + isin(\varphi_b) \end{bmatrix}[A] \tag{2.8}$$

where:

$$\begin{bmatrix} B_1 \\ B_2 \end{bmatrix} = \frac{1}{\sqrt{2}} \begin{bmatrix} 1 \\ 1 \end{bmatrix} [A] \tag{2.9}$$

and

$$\begin{bmatrix} C_1 \\ C_2 \end{bmatrix} = i \begin{bmatrix} sin(\varphi_a) & 0 \\ 0 & sin(\varphi_b) \end{bmatrix} \begin{bmatrix} B_1 \\ B_2 \end{bmatrix} \tag{2.10}$$

are the transfer matrices of the 1×2 MMI symmetric splitter and the differential MZIs, respectively. Here, $A = E_{in} e^{i\omega_c t}$ is the applied input optical field. If the in-phase signal drive V_I is applied to modulator MZM_A and the quadrature signal drive V_Q is applied to modulator MZM_B, i.e.,

$$\begin{aligned} \varphi_a &= \pi \, v_I / v_\pi \\ \varphi_b &= \pi \, v_Q / v_\pi \end{aligned} \tag{2.11}$$

then:

$$\begin{bmatrix} E_1 \\ E_2 \end{bmatrix} = \frac{1}{2} \begin{bmatrix} isin(\pi \, v_I / v_\pi) + sin(\pi \, v_Q / v_\pi) \\ sin(\pi \, v_Q / v_\pi) + isin(\pi \, v_Q / v_\pi) \end{bmatrix} [A] \ . \tag{2.12}$$

For $v_I / v_\pi \ll 1$ and $v_Q / v_\pi \ll 1$, Eq. (2.12) can be written as:

$$\begin{bmatrix} E_1 \\ E_2 \end{bmatrix} \approx \frac{\pi}{2V_\pi} \begin{bmatrix} iv^* \\ v \end{bmatrix} [A] \tag{2.13}$$

where v is the complex modulation $v = v_I + iv_Q$, and $(*)$ stands for the complex conjugate. In the case of a RF modulating signal with amplitude v_{RF}, and angular frequency ω_{RF}, i.e., $v_I = v_{RF} cos(\omega_{RF} t)$, and its companion $\pi/2$ phase-shifted replica, i.e., $v_Q = v_{RF} sin(\omega_{RF} t)$, Eq. (2.13) can be written as:

$$\begin{bmatrix} E_1 \\ E_2 \end{bmatrix} \approx \frac{\pi}{2} \frac{v_{RF}}{v_\pi} \begin{bmatrix} iexp(-i\omega_{RF} t) \\ exp(i\omega_{RF} t) \end{bmatrix} [A] \tag{2.14}$$

and therefore the photonic circuit architecture here described performs as an electrical to optical frequency up-converter with the upper optical side-band available from port E_2 and the lower optical side-band available from port E_1. In principle the optical carrier is entirely suppressed. Eq. (2.14) invokes a small RF signal $m = v_{RF} / v_\pi \ll 1$, a non-necessary condition if recourse is made to the Jacobi-Anger expansion which yields:

$$E_1 = i\frac{1}{2}\left[sin\left(m\pi cos(\omega_{RF}t)\right) - isin\left(m\pi sin(\omega_{RF}t)\right)\right]A = i\sum_{n=0}^{\infty}(-1)^n J_{2n+1}(m\pi)exp[-(-1)^n(2n+1)\omega_{RF}t]\,A \quad (2.15)$$

$$E_2 = \frac{1}{2}\left[sin\left(m\pi cos(\omega_{RF}t)\right) + isin\left(m\pi sin(\omega_{RF}t)\right)\right]A = \sum_{n=0}^{\infty}(-1)^n J_{2n+1}(m\pi)exp[(-1)^n(2n+1)\omega_{RF}t]\,A \quad (2.16)$$

It can be seen from Eq. (2.15) and Eq. (2.16) that all even orders are suppressed, including the carrier. In addition, for port E_2, positive orders equal to $(2n+1)$, with n odd, and negative orders equal to $-(2n+1)$, with n even, are suppressed and vice-versa for port E_1. The principal orders for port E_2 are -3, 1, 5 and for port D_1 are -5, -1, 3, i.e., the optical harmonics alternate between the two output ports.

2.2.2 Frequency Octo-tupling

Using the transfer function in Eq. (2.6), the output of the frequency octo-tupler is given by:

$$D = i\frac{1}{2}\begin{bmatrix}1 & 0\\ 0 & 1\end{bmatrix}\begin{bmatrix}-cos(\varphi_a) & 0\\ 0 & -cos(\varphi_b)\end{bmatrix}\begin{bmatrix}1\\ 1\end{bmatrix}A \quad (2.17)$$

$$= -i\frac{1}{2}[cos(\varphi_a) + cos(\varphi_b)]A \quad (2.18)$$

If the in-phase RF signal is applied to the upper MZI modulator and the quadrature RF signal is applied to the lower MZI modulator as before, then:

$$D = -i\frac{1}{2}\{cos[mcos(\omega_{RF}t)] + cos[msin(\omega_{RF}t)]\}A \quad (2.19)$$

where $m = \pi(v_{RF}/v_{\pi})$. The Jacobi Anger expansion yields:

$$D = -i[J_0(m) + 2J_4(m)\cos(4\omega_{RF}t) + 2J_4(m)\cos(-4\omega_{RF}t) + \dots]A \quad (2.20)$$

Eq. (2.20) indicates the *n-th* order side-bands are suppressed except for n equal to an integer multiple of four. According to the characteristics of the Bessel functions, when the modulation index is $m = 2.40$, the zero-order side-band (i.e. the carrier) is suppressed and the side-bands higher than fourth-order can be ignored without incurring any significant error. When the output of port D is passed through a square-law photo-detector, the circuit performs as a frequency octo-tupler. Other than driving the modulator at $m = 2.40$, the frequency 8-tupling can be achieved by driving the modulator harder ($5.37 \leq m \leq 5.48$)

where the $\pm 4^{th}$ harmonics are significantly higher than the carrier. More details of the analysis of this circuit mode is given in the next chapter.

2.3 Simulation result

VPI software simulation is used to verify the operation of the dual function photonic integrated circuit here proposed. Incoming light is generated by a continuous wave DFB laser diode set at 1550 nm, power of 5 mW, and line-width of 200 kHz. MMIs used are configured as symmetric 1×2 splitters and 2×1 couplers, as well as 2×2 couplers, all with 50 % coupling ratio. Symmetry ensures that the MMI ports have the desired 0 or $\pi/2$ relative phase between output ports (non-ideal cases are discussed later part of the chapter). Ideal phase modulators are used. The switching voltage or half-wave voltage (v_π) of the modulator is simulated first. Half-wave voltage is defined as the applied voltage to a phase modulator for causing a phase change of π (180°), or the voltage required to transition from maximum point to minimum point or minimum point to maximum point in the intensity transmission plot.

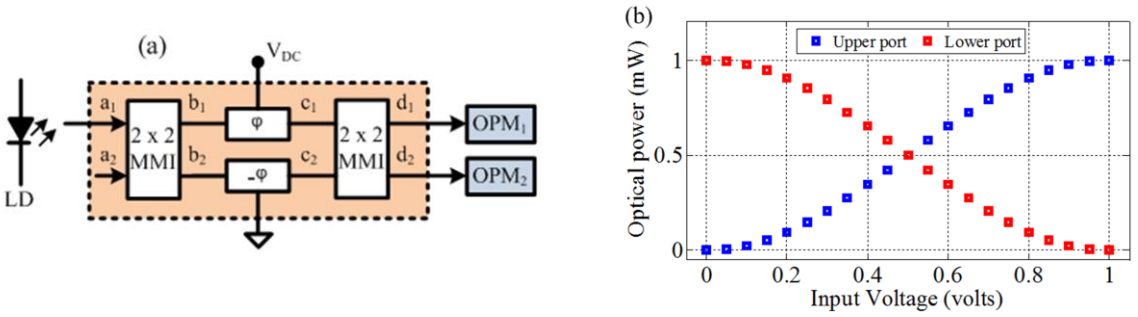

Fig. 2.2. Characterization of MZM; (a) Schematic of the simulated diagram; (b) intensity transmission plot; LD, Laser diode; OPM, Optical power meter.

As shown in Fig 2.2, an optical power of 1 mW is applied at the input of the MZM and a DC-bias is applied to the upper phase modulator while the lower phase modulator is grounded. The output optical power in both the output ports is measured for various DC bias and plotted (as shown in Fig 2.2(b)). The plot shows that the half-wave voltage of the phase modulator is 1V, as 1V is required to transition from maximum to minimum point for lower port and minimum to maximum point for upper port. Hence, lower port is in maximum transmission point (MATP) and upper port is in minimum transmission point (MITP). The switching voltage of the phase modulator is fixed, but if someone drives the MZM

differentially (as shown in Fig 2.3 (a)), means positive DC-bias to the upper modulator and equal and opposite bias to the lower modulator, the transition from maxima to minima and vice versa occurs at half of the switching voltage of a phase modulator.

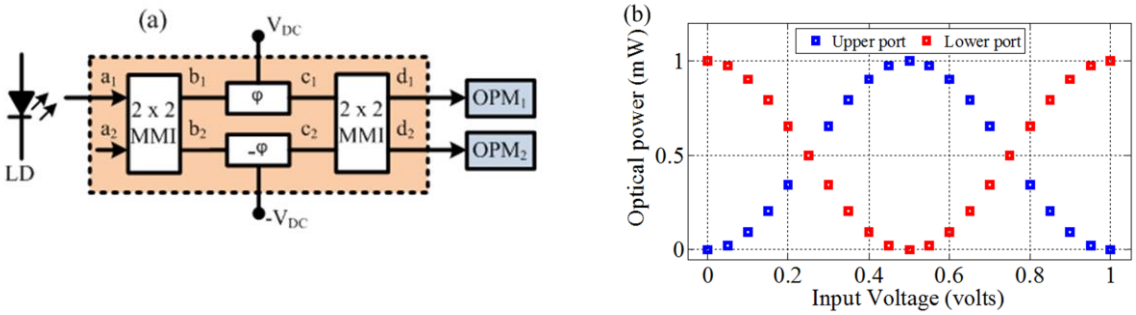

Fig. 2.3. Characterization of MZM; (a) Schematic of the differentially driven MZM; (b) corresponding intensity transmission plot.

For the frequency up-conversion mixer function, a RF driving signal of peak amplitude $v_{RF} = 0.15v_{\pi}$ volts with 60 GHz angular frequency is applied to the four phase modulators with phase relation of 0, $+\pi$, $+\pi/2$ and $-\pi/2$ from top to bottom. Incoming light is generated by a continuous wave DFB laser diode set at 1550 nm, power of 5 mW, and line-width of 200 kHz. In the ideal case, i.e., perfect power split and phase relations among all the MMI ports and the drive signals to the phase modulators with perfect phase relations as specified, a single side band modulation with suppressed carrier is obtained from ports E_1 and E_2 with the upper side band appearing at the upper port and lower side band at the lower port. Fig 2.4 (a) shows the optical spectrum of the resultant upper side-band and lower side-band which verify the theoretical analysis. Both the side-bands at ± 60 GHz are 81 dB higher than the unwanted optical side bands at ∓ 180 GHz. For the frequency 8-tupling generation mode, a 10 GHz RF driving signal of peak amplitude $v_{RF} = 1.73v_{\pi}$ volts without DC-offset is applied to the four phase modulators with relative phase relation mentioned in earlier operation. In the ideal case, Fig 2.4(a) shows the optical spectrum where the $\pm 4^{th}$ harmonic (± 40 GHz) is around 22 dB higher than the optical carrier. Fig 2.4(b) shows the electrical spectrum of the frequency 8-tupled generation where the frequency at 80 GHz (8-tupled of applied 10 GHz RF signal) is 63 dB higher than the unwanted 4^{th} harmonic at 40 GHz frequency.

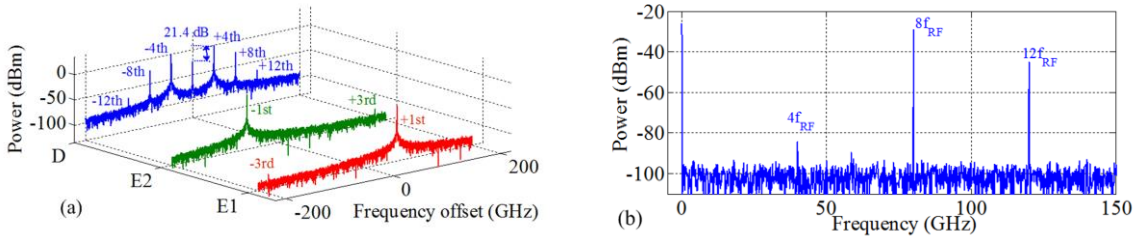

Fig. 2.4. (a) Optical spectra for frequency octo-tupling and frequency up-conversion; (b) Electrical spectrum of the frequency octo-tupled output after square-law photo-detector. The optical noise floor is determined by the laser linewidth while the electrical noise floor is determined by the thermal noise of the photo-diode load. A resolution bandwidth of 156.25 MHz is used for both optical and electrical spectrum analyzer.

Fig 2.5 (a) shows the relationship between peak optical (SSB) and electrical (octo-tupling) power of the harmonics of interest and unwanted harmonics for a wide range of modulation index. It can be seen from Fig 2.5 (b), SSB with 20 dB and above optical side harmonics suppression ratio (SHSR) can be obtained for a wide range of modulation index ($0.01 \leq m \leq 1.409$). It shows that, the operation of SSB modulation does not require carefully adjusted applied RF signal to the phase modulators. On the other hand, for octo-tupling operation, an Electrical SHSR of 20 dB and above is achieved for $m = 2.40$ or $5.37 \leq m \leq 5.48$. It depicts that, frequency multiplication operation requires carefully adjusted modulation index, hence requires careful tuning of the applied RF signal.

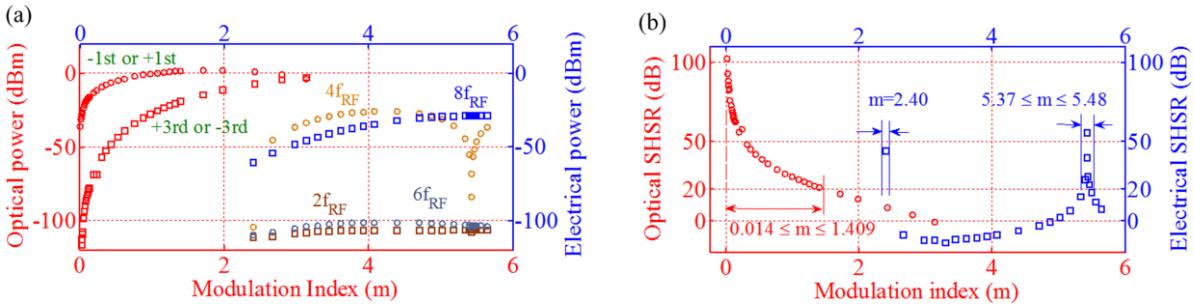

Fig. 2.5. (a) Optical and electrical peak power of the harmonics of interest (circles) and unwanted harmonics for both frequency up-conversion (red colour) and frequency octo-tupling (blue colour). (b) Optical (red colour) and electrical (blue colour) signal of interest to unwanted harmonics for both functionalities.

The performance of the up-converter may deviate from ideal due to power imbalance and phase error between the ports of MMIs. Further deviation may occur due to relative phase errors in the RF signal due to inaccuracy of the waveguide length interconnecting the RF source and phase modulators. To account for these impairments, the performance of the up-conversion mixer and frequency octo-tupling is calculated in terms of optical side harmonic suppression ratio (SHSR) and electrical side harmonics suppression ratio respectively.

Fig 2.6(a) & (b) shows the simulated optical SHSR (up-converter) and electrical SHSR (octo-tupler) for phase error (i.e., deviation from ideal phase) and power imbalances (i.e., deviation from the ideal 50% power split at the input MMIs output ports) at the input MMI. Results show that the phase error and power imbalance has very little impact on the performance of octo-tupler, while the optical SHSR degrades rapidly for frequency up-converter. For 2° phase error the optical SHSR and electrical SHSR are 35 dB and 55 dB respectively, on the other hand these are 40 dB and 45 dB for 2% power imbalance at the input MMI. Similar results are obtained when the phase errors or the power imbalances are mirrored, i.e., $\pm$ phase errors or $\pm$ power imbalance percentages. Furthermore, consistent performance is obtained for the phase errors and power imbalances in other ports of the input MMI coupler of the circuit.

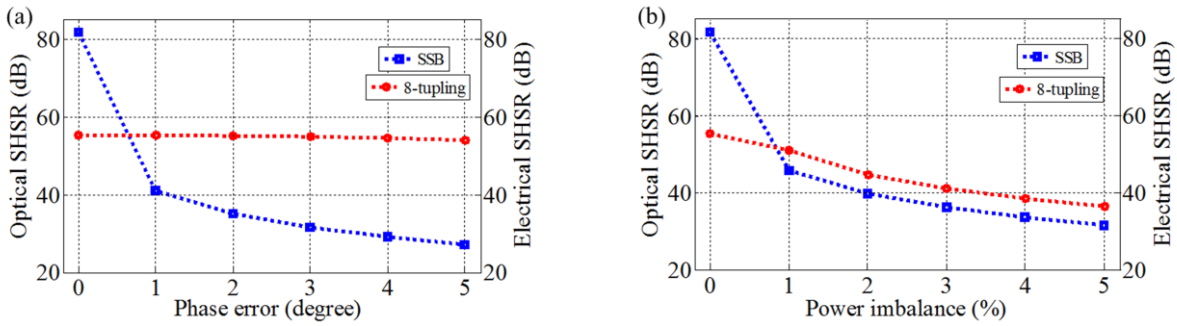

Fig.2.6. Simulated Optical SHSR of the single side band and Electrical SHSR of octo-tupling operation for (a) phase errors and (b) power imbalances in the input 2 × 2 MMI of the Dual-function photonic integrated circuit.

Two types of phase variation is considered in simulation while the RF signal reaching the phase modulators, one is phase error at the input of any phase modulators and others for phase error between two MZIs. Fig 2.7(a)-(b) shows measured SHSR for 0° to 5° phase error

at a single phase modulators and between two MZIs. Simulation result depict an error of 2˚ (i.e., an error of ~1.11% relative to the expected phase of π) at the input of a single phase modulator reduces the SHSR to 40 dB and 26 dB for up-converter and octo-tupler respectively.(Fig 2.7(a)), whereas the same error (but now an error of ~2.22% relative to the expected phase of $\pi/2$) between two MZIs degrades the SHSR little more, numerically 38 dB and 20 dB respectively (Fig 2.8(b)). Identical results are obtained when phase error is mirrored, i.e., $\pm$ phase errors.

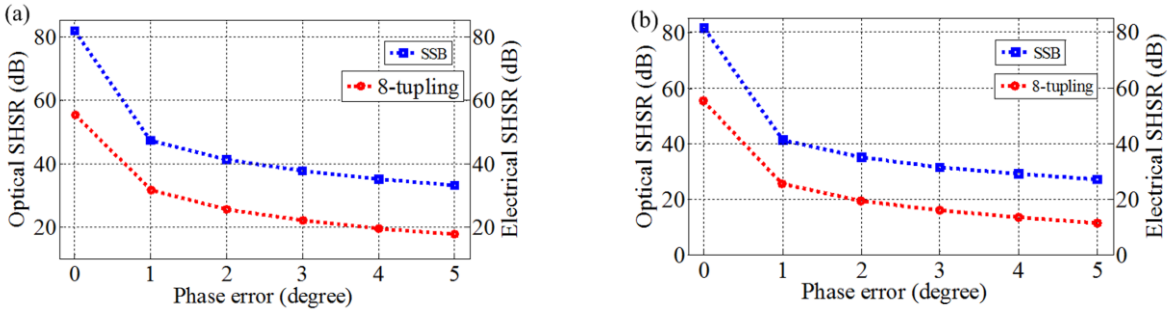

Fig. 2.7. Simulated SHSR of the single side band and frequency octo-tupling operation for phase errors (a) at a single phase modulator and (b) between MZI_A and MZI_B of the Dual-function photonic integrated circuit.

Simulation results show that the length of the waveguides that provide the connection between the RF drive signal and the phase modulators is the critical part of the design compared to the MMIs power imbalances and phase errors between the ports. Furthermore, the power imbalance and phase errors between the ports of a sub-wavelength grating engineered MMI can be substantially reduced compared to a conventional MMI and ensure broadband operation [54]. If required variable trimmer [55] made by small footprint can be implemented to mitigate the imbalances in the phase modulators due to fabrication error.

2.4 Conclusion

In summary, a photonic integrated circuit capable of performing frequency up-conversion of an electrical domain signal to the optical domain and frequency octo-tupling of the RF signal has been proposed and verified by simulation. The proposed architecture can be used as an I & Q modulator also. Furthermore, the circuit requires no DC bias, as the static phase shifts

are introduced using the intrinsic relative phase relations between the output and input ports of MMI couplers. Hence, the design is robust and energy efficient. The SSB operation can be performed for a wide range of modulation index while the frequency octo-tupling is achieved by carefully adjusted modulation index. Finally, due to mature fabrication platforms for MMIs and significantly improving demonstration of phase modulators based on silicon, InGaAsP or hybrid technologies makes the implementation of the dual-function photonic integrated circuit practical.

Chapter 3. Frequency Multiplication: Parallel MZM Configuration

3.1 Introduction

The efficient generation and distribution of millimeter wave (mm-wave) carriers over optical fibers has been an intensive topic of research for various applications and has become one of the key aspects towards the deployment of high-capacity coherent radio-over-fiber systems. Owing to its conceptual simplicity, the remote heterodyne beating of two phase correlated wavelengths impinging onto a high speed photo-receiver is a feasible approach that facilitates the generation of frequency tunable mm-wave carriers. Among different techniques such as optical injection-locking in master-slave laser architectures, and optical-electrical phase loops, the external optical modulation is an attractive and cost effective solution for the creation of two phase correlated wavelengths because their frequency difference can be made equal to an integer factor of the frequency of an electrical local oscillator. Consequently, tunable mm-wave carriers whose frequency is several times larger than that of an electrical local oscillator can be generated. A selected list [29-41] of publications employ a single stage generalized Mach-Zehnder Interferometer (GMZI) architecture in which N phase modulators are interconnected by a 1:N splitter and N:1 coupler. When N is even, the individual phase modulators may be paired and the basic element may be considered to be a dual-drive or most often differential-drive Mach-Zehnder Modulator (MZM).One of the first experimental demonstrations of a frequency doubler based on the remote heterodyne concept was reported over 20 years ago using a single laser source together with a LiNbO3 Mach-Zehnder modulator (MZM) to obtain a narrow line-width 36 GHz electric signal with a peak power around -50 dBm and signal-to-noise ratio (SNR) of over 40 dB [29]. Thereafter, different higher order multiplication factors have theoretically and experimentally been reported, achieving frequency quadrupling [29-32], sextupling [33-34], octo-tupling [35-38] and beyond [39-41]. Regarding frequency quadrupling, for instance, a MZM biased at the maximum transmission point to suppress the odd order side-bands is used in addition with an optical notch filter to generate a 32-50 GHz mm-wave [30] or using an optical filter to generate mm-wave up to 64 GHz [31]. An integrated design comprising two MZM biased at full point and placed in the arms of an

outer MZM biased at the null point is proposed as an optical filter-less approach to obtain second order side bands with an optical and harmonic distortion suppression ratio of more than 36 dB, generating a -30 dBm mm-wave carrier at 40 and 72 GHz [32]. A configuration based on DP-MZM is proposed for frequency sextupling, where the two sub-MZMs are biased at minimum transmission point and the outer MZM is biased at maximum transmission point [33]. Design based on a polarization modulator and wavelength-fixed optical notch filter [34] have been proposed as frequency sextupling approaches to generate tunable carriers from 66 to 114 GHz. Similar designs based on nested MZMs [35] with RF drive adjustment, dual-parallel MZMs (DP-MZM) in combination with notch filters [36], four-parallel phase modulators [37] or two parallel DP-MZM [38] with Y- splitter and combiner at the front and back end have been experimentally and theoretically studied for frequency octo-tupling. Higher frequency multiplication factors have been investigated. For instance, second order harmonics out of a dual-parallel MZM are used to implement degenerate four-wave mixing in a semiconductor optical amplifier to achieve frequency 12-tupling [39]. Two-electrode dual-parallel MZM with carefully adjusted radio frequency drive signals has also been studied and demonstrated by numerical simulations for 12-tupling frequency multiplication [40]. A configuration of three MZM in parallel has been proposed for frequency 6-tupling, 12-tupling, and 18-tupling depending upon the bias conditions on the modulators [41]. A constant feature in almost all the above mentioned reports is the use of discrete components, the need of bias points as well as large and carefully adjusted drive signals going to the MZMs, and optical filtering stages to suppress the optical carrier or unwanted harmonics. Hence, frequency multiplication integrated design with multiplication factor 6 and above that overcoming the drift caused by dc-voltages and the elimination of optical filters remains challenging. In this chapter, a theoretical analysis is developed for a generalized architecture having N parallel phase modulators driven electrically with a progressive $2\pi/N$ phase shift. The theoretical analysis depicts that, any unwanted harmonics can be fully suppressed while maximizing the harmonics of interest by carefully selecting the static optical phase shifts required in each of the N parallel arms. The phase modulators of the architecture can be rearranged to form equivalent parallel MZM structure for even N. Commercially available software is used to justify the theoretical prediction for N=8 architecture with properly determined optical phase shifts to generate high orders harmonics

(±4) in the optical domain separated by $8f_{RF}$, where f_{RF} is the RF frequency. Results in frequency multiplication of the electrical signal once pass through the photo-detector. Furthermore, it is shown that the above mentioned static optical phase shift can be removed by taking the advantage of the phase relationship between the input and output signal in the 4×4 MMI couplers. The proposed circuit overcomes some of the previously reported frequency 8-tupling architectures because it requires no dc bias and its operation is not restricted to relatively large and carefully adjusted modulation indexes for suppression of unwanted harmonics. As a theoretical prediction, transfer matrix approach is used to describe the operation of the frequency 8-tupling and 24-tupling. The concept is validated by computer simulations. Along with ideal scenario, imperfect state such as power imbalances in the multi-mode interference couplers, imperfect phases of the electric drives to the phase modulators are analyzed. The proposed approach anticipates Si- or III-V or hybrid integration technologies given the development of linear electro-optic modulator technology. In addition to that, a functionally equivalent circuit that uses traditional MZM on LiNbO3 platform is proposed. Theoretical and simulation analyses are also presented. Finally, a comparison is presented between our proposed architecture and architecture based on traditional MZM to validate the performances.

3.2 Theoretical Analysis

Consider an array of N phase modulators in parallel as shown in Figure 3.1, where each modulator is electrically driven by a progressive phase shift in units of 2π/N. The complex amplitude of the field at the output of each PM can be expressed by using the Jacobi- Anger expansion:

$$\exp\left[im\cos\left(\theta + p\frac{2\pi}{N}\right)\right] = \sum_{n=-\infty}^{\infty}\left[\exp\left(ipn\frac{2\pi}{N}\right) i^n J_n(m)\exp(in\theta)\right] \quad (3.1)$$

where m is the modulation index; $\theta = \omega t$ and $p\,2\pi/N$ are the dynamic and static phase of the electrical drive signal; p is a positive integer, denotes the index of the phase modulator in the array starting from top to bottom; $J_n(\cdot)$ is the Bessel function of the first kind with order n, and $i = \sqrt{-1}$ is the imaginary number.

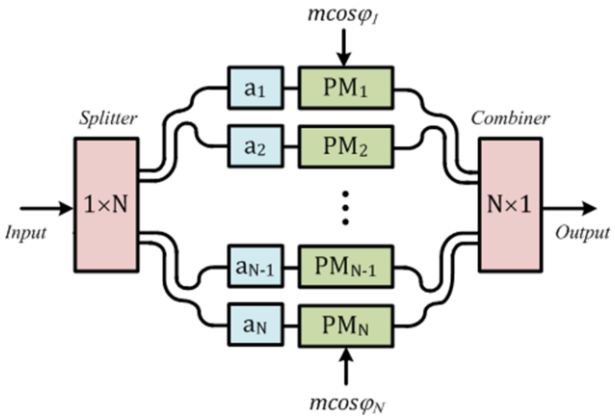

Fig. 3.1. Schematic diagram of a generalized Mach-Zehnder interferometer consisting of an array of *N* phase modulators in parallel between a splitter and combiner.

The output of the combiner is:

$$\frac{1}{N}\sum_{p=0}^{N-1}\left[a_p \exp\left(imcos\left(\theta + p\frac{2\pi}{N}\right)\right)\right] = \sum_{n=-\infty}^{\infty}[\tilde{a}_n i^n J_n(m) exp(in\theta)] \quad (3.2)$$

where $\tilde{a}_n$ can be represented as the discrete Fourier transform:

$$\tilde{a}_n = \frac{1}{N}\sum_{p=0}^{N-1}\left[a_p exp\left(ipn\frac{2\pi}{N}\right)\right] \quad (3.3)$$

The sequence a_p denotes the space domain complex weight of each phase modulator, which is preferably uni-modular to minimize loss of energy, i.e., a phase shift. It is observed that the sequence $\tilde{a}_n$ is periodic with period *N*. The importance of equations (3.2) and (3.3) can be understood by considering first the simplest case for the weights, which is

$$a_p = 1 \qquad \forall \quad p = 0,1,\dots,N-1. \quad (3.4)$$

Let us consider,

$$z = exp(iq\,2\pi/N) \quad (3.5)$$

The sum of the geometric series is given by:

$$\sum_{p=0}^{N-1} z^p = (1 - z^N)/(1 - z) \quad (3.6)$$

The discrete Fourier transform term (3.3) may then be evaluated to yield:

$$\tilde{a}_n = \frac{1}{N}\frac{1-exp(in2\pi)}{1-exp\left(in\frac{2\pi}{N}\right)} = \frac{1}{N} exp\left[in\left(\frac{N-1}{N}\right)\pi\right]\frac{sin(n\pi)}{sin\left(n\frac{\pi}{N}\right)} \quad (3.7)$$

Applying L'Hôpital's rule to equation (3.7), it is found that $\tilde{a}_0 = 1$ for $n = 0$, and $\tilde{a}_n = 0$ for $n = 1,2, \ldots, N-1$. The frequency domain sequence therefore supresses periodically all harmonics except those that are multiples of *N*. One may take advantage of the shift theorem by modifying a given set of weights by the application of a progressive phase factor with increment $-n_0\, 2\pi/N$. That is

$$a_p \rightarrow a_p exp(-ipn_0\, 2\pi/N)$$

and hence:

$$\tilde{a}_n \rightarrow \frac{1}{N}\sum_{p=0}^{N-1}\left[a_p exp\left(ip(n-n_0)\frac{2\pi}{N}\right)\right] = \tilde{a}_{n-n_0} \tag{3.8}$$

Therefore the origin of the weights can be shifted to position n_0 by a progressive phase shift of the light exciting the phase modulators with increment$-n_0\, 2\pi/N$. For the special case $a_p = 1$ and integer n_0, $\tilde{a}_{n-n_0}$ is zero for each order except $n = n_0 + lN$, where l is an integer. Hence, the proposed design approach suppresses specific harmonic orders while maximising the harmonic orders of interest. Since the process does not depend upon the modulation index, the linearity of the *N*-parallel phase modulators array is maintained and each PM can be driven at moderate input powers. Furthermore, for an even (multiple of four) number of phase modulators, there will be pairs of differentially driven phase modulators, leading to an equivalent parallel MZM interpretation. As mentioned earlier, any harmonics can be maximized (single side-band modulation, frequency multiplication) while other can be suppressed, in this chapter the design of frequency multiplication of electrical signal will be discussed only. Specifically, an array consist of eight (8) phase modulator for generating frequency multiplication is discussed in following section to validate the design methodology.

3.2.1 Array of 8 Phase Modulators

The schematic diagram of a generalized Mach-Zehnder interferometer consisting of an array of eight phase modulators (N = 8) is shown in Figure 3.2, with progressive electrical phase shifts φ_p equal to 0, $\pi/4$, $\pi/2$, $3\,\pi/4$, π, $5\pi/4$, $3\,\pi/2$, and $7\pi/4$ respectively. To achieve frequency octo-tupling, the coefficient $q_0 = \pm 4$ and the lowest order unsuppressed harmonics are ± 12 and ± 20. In this case, the required optical weights a_p also have a progressive phase shifts of 0, π, 0 π, 0, π, 0, and π respectively.

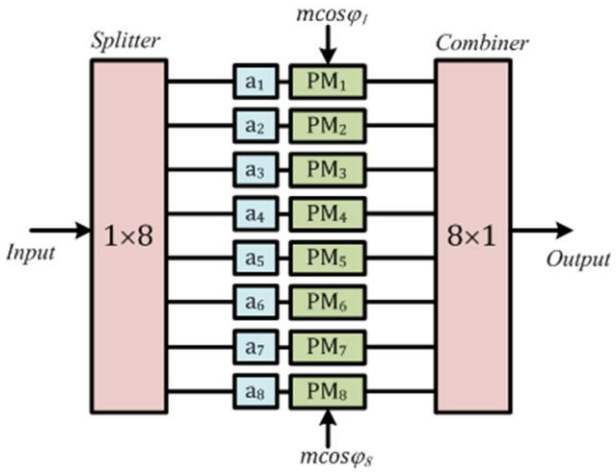

Fig. 3.2. Schematic diagram of a generalized Mach-Zehnder interferometer consisting of an array of 8 phase modulators.

When all the phase modulators are re-ordered to form MZM with pair of differentially driven phase modulators, then the optical static phase required for the four MZM are 0, π, 0 and π, respectively. Table 3.1 summarizes the required electrical and optical phase shifts for the frequency multiplication design.

Table 3.1 Design conditions and obtained operation in an array of 8-parallel phase modulators.

When all the PM are in parallel having $2\pi/N$ progressive electrical phase shift				When PM are re-ordered to form differentially driven MZMs		
Conditions and obtained operation	PM-index	Phase shift		MZM-index	Phase shift	
		Optical	Electrical		Optical	Electrical
(a) $n_0 = \pm 4$ $n =$ $\{\cdots$ $-12, -4, +4, +12 \cdots\}$ Frequency octo-tupling	0	0	0	1	0	0
	1	π	π/4		0	π
	2	0	π/2	2	π	π/4
	3	π	3π/4		π	5π/4
	4	0	π	3	0	π/2
	5	π	5π/4		0	3π/2
	6	0	3π/2	4	π	3π/4
	7	π	7π/4		π	7π/4

By careful exploiting the intrinsic phase relations between the outputs ports of the MMI couplers connected to the phase modulators, the required static optical phase shift may be avoided. In our case, taking advantage of the phase relationships between the input and output signals in the 4×4 MMI coupler and combiner [18], as well as the above mentioned relative phase of the electrical local oscillator driving the phase modulators, it is theoretically shown that the photonic circuit performs the 8-fold multiplication of the electric local oscillator frequency. The front- and back-end of the proposed circuit comprises 4×4 multi-mode interference (MMI) couplers enclosing an array of four pairs of phase modulators and 2×2 MMI couplers. A schematic diagram of the newly revised photonic circuit is illustrated in Figure 3.3(a).The photonic circuit architecture here presented comprises eight phase modulators situated in the arms between an interconnected 4×8 distribution tree and a complementary 8×4 combination tree. The 4×8 distribution tree is formed by an outer stage consisting of a 4×4 MMI coupler followed by an inner stage consisting of parallel pairs of 2×2 MMI couplers, each with one complementary port unused.

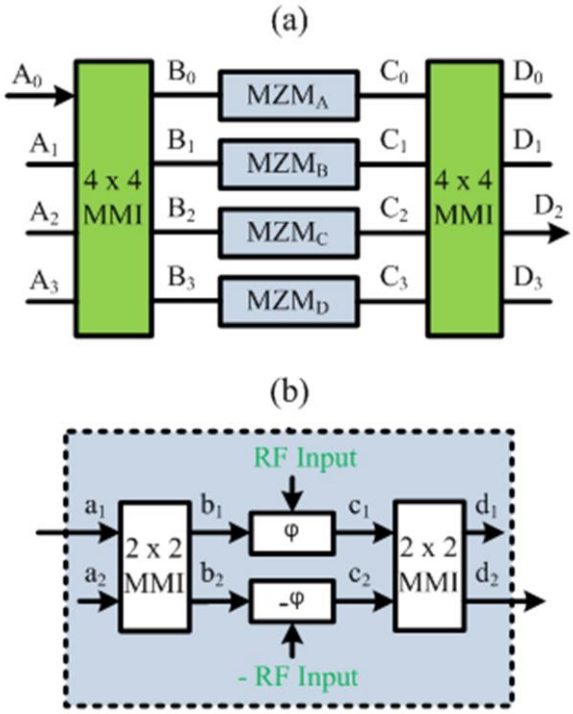

Fig. 3.3 (a) Schematic diagram of the proposed frequency 8-tupling and 24-tupling multiplication circuit. (b) Mach-Zehnder Interferometer driven differentially.

The 8×4 combination tree is a reciprocal structure of the distribution tree. As shown in Figure 3.3(b), each pair of phase modulators is combined with the inner stage of 2×2 MMIs. This Mach-Zehnder Interferometer arrangement performs as a standard MZM when driven differentially. For given phase relations of the drive signal reaching each phase modulator, the upper and lower output ports of the MZMs produce odd and even harmonics (including the optical carrier), respectively. Owing to the complementary phases between the intermediate output ports d_2 in the four MZMs and the phase relationships of the output 4×4 MMI, constructive and destructive interference produce $\pm$4-th harmonics with optical carrier suppression in port D_2. After photo detection, the photonic circuit here proposed performs the 8-fold and 24-fold multiplication of the local oscillator frequency driving the phase modulators.

The output of the high order frequency multiplication circuit can be obtained by using the transfer matrix for each element in Figure 3.3. The transfer matrix for each $MZM_{A,B,C,D}$ is as follows:

$$\begin{bmatrix} d_1 \\ d_2 \end{bmatrix} = i \begin{bmatrix} sin(\varphi) & -cos(\varphi) \\ -cos(\varphi) & -sin(\varphi) \end{bmatrix} \begin{bmatrix} a_1 \\ a_2 \end{bmatrix} \tag{3.9}$$

where $\varphi = \pi\, v/v_\pi$ is the optical phase shift impressed to the phase modulator of a MZM with switching voltage of v_π by the application of a differential signal with amplitude v. Using Equation (3.9) and assuming ports a_2 and d_1 are unused for the target application, the output of the circuit can be represented by:

$$d_2 = -i\cos(\varphi) a_1 \tag{3.10}$$

$$\begin{bmatrix} D_0 \\ D_1 \\ D_2 \\ D_3 \end{bmatrix} = -i[T] \begin{bmatrix} cos\varphi_A & 0 & 0 & 0 \\ 0 & cos\varphi_B & 0 & 0 \\ 0 & 0 & cos\varphi_C & 0 \\ 0 & 0 & 0 & cos\varphi_D \end{bmatrix} [T] \begin{bmatrix} A_0 \\ A_1 \\ A_2 \\ A_3 \end{bmatrix} \tag{3.11}$$

where:

$$T = \frac{1}{\sqrt{4}} \begin{bmatrix} 1 & \zeta & -\zeta & 1 \\ \zeta & 1 & 1 & -\zeta \\ -\zeta & 1 & 1 & \zeta \\ 1 & -\zeta & \zeta & 1 \end{bmatrix} \tag{3.12}$$

is the transfer matrix of the 4×4 MMI coupler and combiner, with $\zeta = e^{i\pi/4}$ [18] and $\varphi_{A,B,C,D}$ are the optical phase shifts of each $MZM_{A,B,C,D}$ respectively. Developing (3.11) and (3.12), the output in port D_2 is expressed as:

$$D_2 = \frac{-iA_0\zeta}{4}(-cos\varphi_A + cos\varphi_B - cos\varphi_C + cos\varphi_D) \tag{3.13}$$

Assuming the signals $v_n = v_{RF}cos(\omega_m t + \theta_n)$ driving each MZM have a progressive $\pi/4$ phase shift and using the Jacobi-Anger expansion, each term in (3.13) can be represented as

$$cos\big(mcos(\omega_m t)\big) = J_0(m) + 2\sum_{n=1}^{\infty}(-1)^n J_{2n}(m)cos(2n\omega_m t) \tag{3.14}$$

$$cos(mcos(\omega_m t) + \pi/4) = J_0(m) + 2\sum_{n=1}^{\infty}(-1)^n J_{2n}(m)cos(2n\omega_m t + n\,\pi/2) \tag{3.15}$$

$$cos(mcos(\omega_m t) + \pi/2) = J_0(m) \quad +2\sum_{n=1}^{\infty}(-1)^n J_{2n}(m)cos(2n\omega_m t + n\pi) \tag{3.16}$$

$$cos(mcos(\omega_m t) + 3\pi/4) = J_0(m) + 2\sum_{n=1}^{\infty}(-1)^n J_{2n}(m)cos(2n\omega_m t + 3n\pi/2) \tag{3.17}$$

Developing the right-hand side terms in Equations (3.14) to (3.17), substituting them into Equation (3.13) and eliminating common terms, the signal at the output port D_2 can be reduced to:

$$D_2 = i2A_0\zeta[J_4(m)\cos(4\omega_m t) + J_4(m)\cos(-4\omega_m t) + J_{12}(m)\cos(12\omega_m t) + J_{12}(m)\cos(-12\omega_m t) + \cdots] \tag{3.18}$$

where $m = \pi\, v_{RF}/v_\pi$ is the modulation index of the MZMs, and $J_n(\cdot)$ is the Bessel function of first kind with order n. From Equation (3.18), it can be seen that all the n-th order side bands are suppressed, except those for $n = 4x$, where x is an odd integer. Moreover, for modulation indexes $m \leq 6.5$, only the terms $J_4(m)$ are non-negligible and hence the circuit performs as a frequency 8-tupling after the output is passed through a square-low photo-diode. Note for modulation index around 11, the term $J_{12}(m)$ becomes dominant and eventually the circuit can perform the frequency 24-tupling of an electric local oscillator.

3.2.2 Two Parallel DP-MZM

The realization of the same function by using the traditional MZM configuration, which uses the $LiNbO_3$ integration technology, the most mature platform is proposed in the following section.

The proposed circuit architecture, shown in Figure 3.4, is formed by an outer Mach-Zehnder interferometer (MZI) biased at its MITP with each of its two arms containing a pair of

MZMs in parallel; each biased at its MATP. Both the MZM are driven by in-phase and quadrature RF signals. Each arm generates optical sidebands with orders equal to an integer multiple of four. When combined by the outer MZI, the orders equal to an even integer multiple of four are suppressed; only orders equal to an odd integer multiple of four ($\pm 4, \pm 12, \pm 20 \ldots$) are unsuppressed.

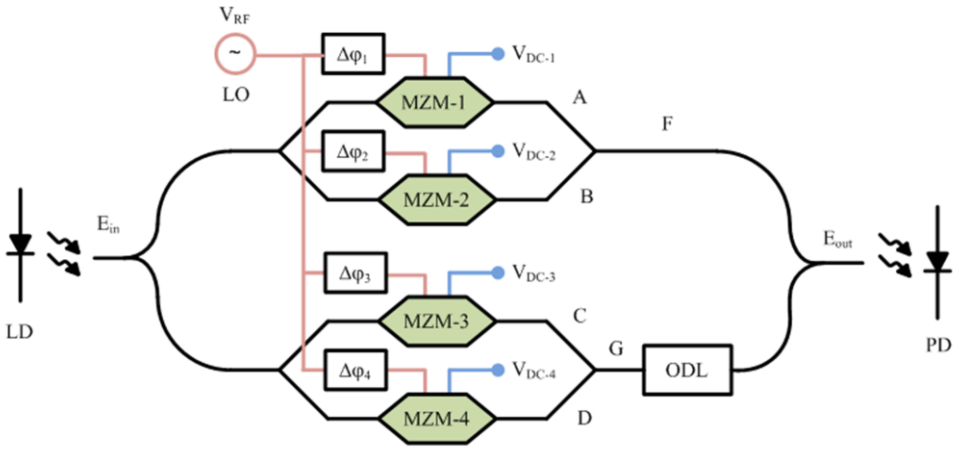

Fig. 3.4. Millimetre wave generation by frequency multiplication using two parallel DP-MZMs with an optical delay line. LD: laser diode; LO: RF local oscillator; PD: photodiode; ODL: optical delay line; MZM: Mach-Zehnder modulator.

As all the MZMs are biased at their maximum transmission point and hence their (ideal) amplitude transmission functions h is:

$$h(t) = cos\left[m\, cos\left(\omega_{RF} t + \Delta\varphi_p\right)\right] \tag{3.19}$$

If the RF phase shifts are set to $\Delta\varphi_1 = 0$, $\Delta\varphi_2 = \pi/2$, $\Delta\varphi_3 = \pi/4$ and $\Delta\varphi_4 = 3\,\pi/4$, the outputs at nodes A,B,C,D respectively are:

$$\begin{gathered} cos[mcos(\omega_{RF} t + \Delta\varphi_1)] = \\ J_0(m) - 2J_2(m)\, cos(2\omega_{RF} t) + 2J_4(m)\, cos(4\omega_{RF} t) - 2J_6(m)\, cos(6\omega_{RF} t) \\ +2J_8(m)\, cos(8\omega_{RF} t) - 2J_{10}(m)\, cos(10\omega_{RF} t) + 2J_{12}(m)\, cos(12\omega_{RF} t) \cdots \end{gathered} \tag{3.20}$$

$$\begin{gathered} cos[mcos(\omega_{RF} t + \Delta\varphi_2)] = \\ J_0(m) + 2J_2(m)\, cos(2\omega_{RF} t) + 2J_4(m)\, cos(4\omega_{RF} t) + 2J_6(m)\, cos(6\omega_{RF} t) \\ +2J_8(m)\, cos(8\omega_{RF} t) + 2J_{10}(m)\, cos(10\omega_{RF} t) + 2J_{12}(m)\, cos(12\omega_{RF} t) \cdots \end{gathered} \tag{3.21}$$

$$cos[mcos(\omega_{RF}t + \Delta\varphi_3)] =$$
$$J_0(m) + 2J_2(m)\,sin(2\omega_{RF}t) - 2J_4(m)\,cos(4\omega_{RF}t) - 2J_6(m)\,sin(6\omega_{RF}t) \quad (3.22)$$
$$+2J_8(m)\,cos(8\omega_{RF}t) + 2J_{10}(m)sin(10\omega_{RF}t) - 2J_{12}(m)\,cos(12\omega_{RF}t)\cdots$$

$$cos[mcos(\omega_{RF}t + \Delta\varphi_4)] =$$
$$J_0(m) - 2J_2(m)sin(2\omega_{RF}t) - 2J_4(m)\,cos(4\omega_{RF}t) + 2J_6(m)\,sin(6\omega_{RF}t) \quad (3.23)$$
$$+2J_8(m)\,cos(8\omega_{RF}t) - 2J_{10}(m)\,sin(10\omega_{RF}t) - 2J_{12}(m)\,cos(12\omega_{RF}t)\cdots$$

The output at node F obtained from equations (3.20) and (3.21) is:

$$E_F \sim J_0(m) + 2J_4(m)\,cos(4\omega_{RF}t) + 2J_8(m)\,cos(8\omega_{RF}t) + 2J_{12}(m)\,cos(12\omega_{RF}t) + \cdots \quad (3.24)$$

The output at node G obtained from equations (3.22) and (3.23) is:

$$E_G \sim J_0(m) - 2J_4(m)\,cos(4\omega_{RF}t) + 2J_8(m)\,cos(8\omega_{RF}t) - 2J_{12}(m)\,cos(12\omega_{RF}t) + \cdots \quad (3.25)$$

The optical delay line inverts the sign of the terms in Equation (3.25) and hence the final output is:

$$E_{out}/E_{in} = 2J_4(m)\,cos(4\omega_{RF}t) + 2J_{12}(m)\,cos(12\omega_{RF}t) + \cdots \quad (3.26)$$

Equation (3.26) is similar as Equation (3.18), which validates both the design. The terms $J_{12}(m)$ are negligible for modulation indexes $m \leq 6.5$ and the circuit functions as a frequency octupler on passing the output to a photodiode. On the other hand, if it is permissible to adjust the modulation index, then frequency 24-tupling can be achieved from the same architecture by setting $J_4(m) = 0$, i.e. a modulation index $m = 11.06\ or\ 14.37$. Moreover any reversible 2×2 splitter / coupler that have mirror symmetry about a plane bisecting its input and output ports (i.e. a 2×2 multi-mode interference coupler (MMI) or directional coupler) has an intrinsic $\pi/2$ phase difference between its ports. The π phase change may then be implemented by replacing the 1×2 $y-$branch splitter that feeds light into, and 2×1 $y-$branch that combine light from the two DP-MZMs, by mirror symmetric arrangements of a 2×2 splitter with one input port left unused and a 2×2 combiner with one output port unused. Hence the use of optical delay line can be avoided. The proposed design may be implemented as a quick check by using commercially available two parallel DP-MZM as the fabrication process of the photonic integration will take time.

3.3 Simulation Results

The operation of the proposed design in this chapter is demonstrated by implementing computer simulations in Virtual Photonics Inc. (VPI) software package (Version 9.1). A continuous wave DFB laser diode set at a wavelength of 1550 nm with a line-width of 200 kHz and power of 10 mW is used as the optical input. Ideal phase modulators are used. For the verification of 8-parrallel phase modulator array to implement frequency multiplication, optical phase shifters are used to model the uni-modular complex coefficients a_p, whereas cascaded Y-branches are used as the 1×8 input splitter and 8×1 output combiner. A 7.5 GHz sinusoidal drive signal is applied to the phase modulators. Since the circuit operation is not restricted to carefully adjusted amplitude of the drive signal, modulation indexes from 2.5 to 7.5 can be set. As an illustrative example for maximised frequency 8-tupling, the modulation index is set to $m = 5.28$, which results in an amplitude of $1.68\,V$ for phase modulators with $v_\pi = 1\,V$. The phase of the drive signals at the input of the eight phase modulators (from top to bottom) is set to according to Table I. As shown Fig 3.5, 4-th harmonics at ± 30 GHz (4×7.5 GHz) without optical carrier are obtained.

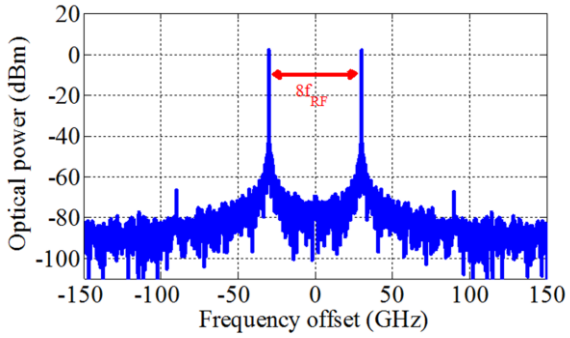

Fig. 3.5. Optical spectrum of the simulated circuit mentioned in Fig 3.2.

In a similar way, 4×4 and 2×2 MMIs are configured as couplers and splitters with proper power and phase relations according to the self-imaging principle [hamdam] to implement the proposed design in Figure 3.5. The phase of the drive signals at the input of the eight phase modulators (from top to bottom) is set to 0 & π (MZM_A), $\pi/4$ & $5\pi/4$ (MZM_B), $\pi/2$ & $3\pi/2$ (MZM_C) and $3\pi/4$ & $7\pi/4$ (MZM_D). The peak amplitude and frequency of the RF signal is kept same as above.

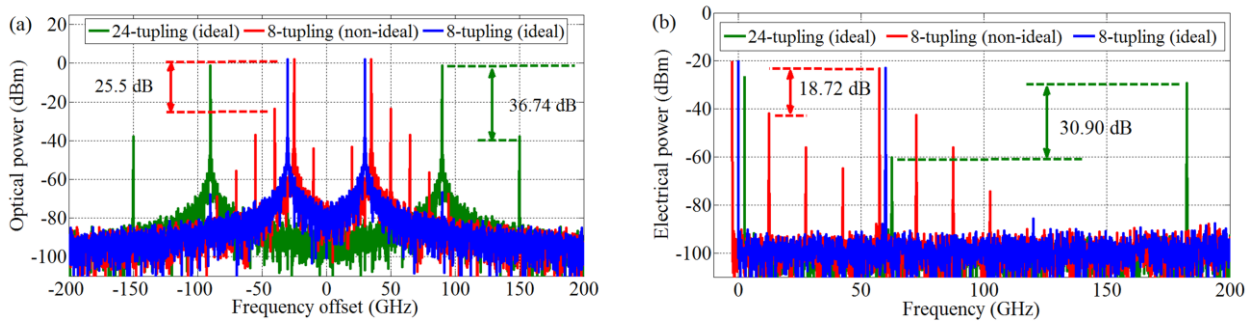

Fig. 3.6. (a) Optical spectrum of the signal at output port D_2. (b) Electrical spectrum after photo detection. For visualization, plots for 24-tupling (ideal) and 8-tupling (non-ideal) have been frequency shifted by ±2 GHz.

In the ideal case of perfect power split and phase relations among all the MMI ports and above mentioned phase relations of the drive signals applied to the phase modulators, frequency 8-tupling is achieved. As shown Fig 3.6(a), 4-th harmonics at ± 30 GHz (4×7.5 GHz) without optical carrier and over 69 dB suppression ratio from unwanted harmonics are obtained. After photo-detection, a clean frequency component at 60 GHz with electrical side harmonic suppression ratio (ESHSR) of over 65 dB is obtained and shown in Fig 3.6(b), achieving thus the 8-fold frequency multiplication of the input drive signal. To take into account practical inaccuracies such as minor phase errors and power imbalances in the design or fabrication of the MMIs, as well as the lengths of the waveguides interconnecting the various components in the proposed photonic circuit, the performance of the frequency 8-tupled signal is analyzed in non-ideal conditions. The ESHSR that is obtained after accounting for power imbalances in port B_0 of the input 4×4 MMI from ideal to 10 % is shown in Fig 3.6(c). Similar performance is obtained in the simulations for power imbalances in other ports of the input 4×4 MMI. The operation of the 8-tupling circuit taking into account phase errors from 0° (ideal case) to 10° in both a single phase modulator (i.e., $0 \pm 10°$ in the top phase modulator) and in a differential MZM (i.e., $(0 \ \& \ \pi) \pm 10°$ in MZM_A) is shown in Fig 3.6(c). As also discussed in earlier chapter, simulation results indicate the appearance of unwanted harmonics arises at a larger extent due to the phase errors in the drive signals reaching the differential modulators. The length of the waveguides connecting the drive signal to the phase modulators can hence be considered as the critical design point in the proposed photonic circuit. Nevertheless, an EHDSR of over 30 dB is

obtained for 5% error in the 4 × 4 MMI power imbalance and over 18 dB for 5° phase error in the drive signals, overcoming previously reported values for 8-fold frequency multiplication.

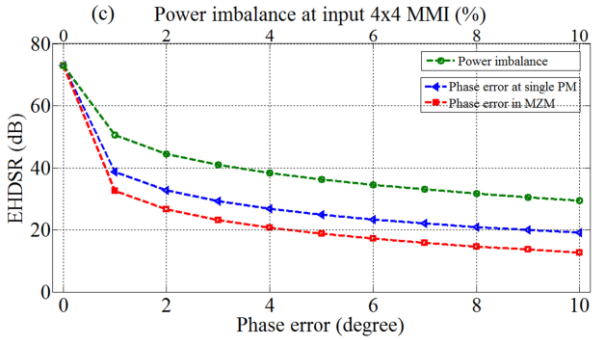

Fig. 3.6(c). ESHSR for power imbalances in the input 2 × 2 MMI and phase errors in the phase modulators.

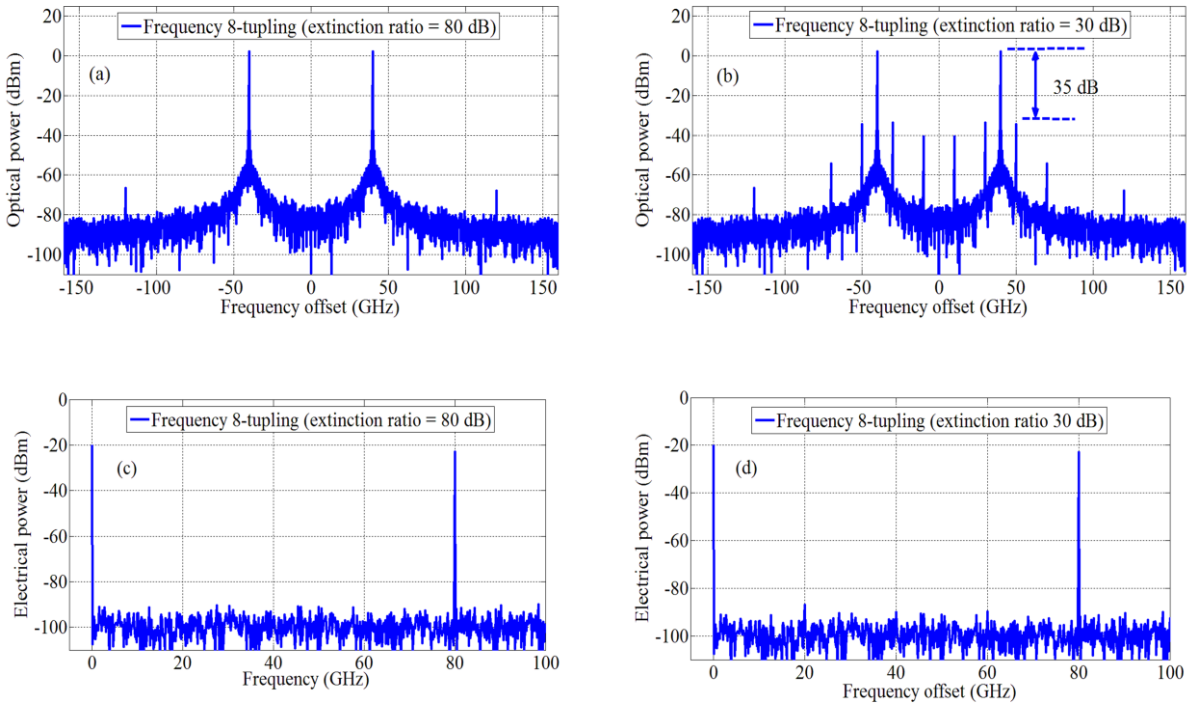

Fig. 3.7. Optical (a)-(b) and electrical spectrum (c)-(d) of a frequency 8-tupling based on the proposed modified structure. Both 80 dB (infinite) and 30 dB extinction ratio in the MZMs are considered in the simulations.

Further simulation verification is presented for the proposed design in Figure 3.4 based on the traditional MZM. The phase modulator half-wave voltage v_π used is 5V, which is the representative of commercially available $LiNbO_3$ modulators. The frequency of the RF drive signal is set to 10 GHz. It can be seen from the Figure 3.7 that the simulation results completely agree with the analysis presented herein. A pristine electrical spectrum is produced without any unwanted harmonics for MZMs with infinite extinction ratio (i.e., set to 80 dB in VPI) and remains pristine for an extinction ratio reduced to 30 dB. It is shown from the simulation result that both the architecture perform identical result. Furthermore, all the possible impairments that may happen in practical are taken into account and a comparison is presented between the traditional MZM architecture and with the newly proposed idea in tabular from. The extinction ratio of the MZM used is 30 dB. The comparison shows that both the architecture provides almost same ESHSR when different kinds of impairments are applied. Hence, the result justifies the performance of the newly proposed method with traditional MZM circuit.

Table 3.2 The performance comparison between traditional MZM architecture and newly proposed architecture.

Impairments'		Proposed structure ESHSR (dB)	Traditional MZM structure ESHSR (dB)	Error (%)
Input power imbalance (%)	1	50.57	50.38	0.37
	2	44.53	44.61	0.18
	3	40.99	41.15	0.39
	4	38.31	38.69	0.99
	5	36.24	36.76	1.43
RF phase error at single PM (degree)	1	38.63	38.04	1.53
	2	32.67	32.24	1.31
	3	29.18	28.82	1.23
	4	26.73	26.40	1.23
	5	24.83	24.53	1.20
RF phase error between MZM (degree)	1	32.65	32.46	0.58
	2	26.66	26.56	0.38
	3	23.15	23.07	0.35
	4	20.65	20.59	0.29
	5	18.73	18.67	0.32

3.4 Conclusion

In summary, a theoretical approach based on Nparallel phase modulators driven with progressive electrical $2\pi/N$ phase shift is presented. A simulation verification of the theoretical prediction is presented for 8 phase modulators which can be used for implementing frequency 8-tupling by carefully choosing the static optical phases. To overcome the requirement of static optical phase shift, a new design is proposed that uses the phase relation among the ports of 4×4 MMI. The proposed design overcomes previously reported works because the frequency multiplication scheme requires no optical or electrical filters, the operation is not limited to carefully adjusted modulation indexes, and the drift originated from static dc bias is mitigated by making use of the intrinsic phase relations of multi-mode interference couplers. After analyzing the simulation results, the frequency 8-tupling and 24-tupling with optical carrier and harmonic distortion ratio of over 30 dB is achieved for inaccuracies on the 5% power imbalance of the input MMI and over 18 dB for 5° phase errors on the drive signals. Furthermore, a functionally equivalent circuit that uses traditional MZM based on $LiNbO_3$ technology is demonstrated and finally, a comparison is presented with our designed circuit. Comparison shows that both the circuit's performances are same. The implementation of the proposed frequency multiplier in a photonic integrated circuit seems feasible because of the mature fabrication platforms for MMIs and the rapidly advancing demonstrations of phase modulators based either on silicon, InGaAsP, silicon-organic materials, or hybrid integration technologies.

Chapter 4. Frequency Multiplication: Cascade MZM Configuration

4.1 Introduction

Optical millimeter wave generation is one of the key techniques towards the deployment of coherent radio-over-fiber systems. Amongst various techniques to optically generate widely-tunable mm-wave signals, a conceptually simple approach is the heterodyne beating of two phase correlated optical carriers separated in wavelengths at a high speed photo-detector. Although there are different techniques can be used to generate phase correlated optical carriers, the external modulation of a laser is an attractive and cost effective solution as the technique offers highly stable spectrally-pure tunable mm-wave carrier with system simplicity. As a consequence, mm-wave carriers having frequency lager than that of an electrical local oscillator can be generated.

Numerous circuit architectures have been conceived [29-47] that contain several phase modulators driven from the same optical and electrical sources but with carefully chosen relative phase-shifts combined in a network such that only two optical lines separated by a desired multiple of the RF frequency have significant amplitude at the output port. The majority of the circuits proposed [29-42] employ essentially a single stage generalized Mach-Zehnder Interferometer (GMZI) architecture in which N phase modulators are interconnected by a 1:N splitter and N:1 coupler. When N is even, the individual phase modulators may be paired and the basic element may be considered to be a dual-drive or most often differential-drive Mach-Zehnder Modulator (MZM). Circuit designs for frequency multiplication by quadrupling [29-32] & [42-43, 46], sextupling [33, 44, 47], octo-tupling [35-38, 45-46] and by greater factors [39-41] have been reported. The use of discrete components; the need for static DC bias points; and the use of carefully adjusted electrical drive levels or optical filtering to suppress a particular unwanted harmonic are among the most common demerits of these designs. A notable advance is reported in the previous chapter, where a DC bias-less and filters-less frequency octo-tupler free of any requirement to set a precise electrical drive level is presented.

A lesser number of proposals have considered two-stage architectures in which the basic element, i.e., MZMs, are connected in series [42-46] or both in series and parallel [47].Circuit designs for frequency multiplication by quadrupling, sextupling and octo-tupling using two-stage cascade MZM structure are proposed in references [42-46]. The MZM modulators are biased at the minimum transmission point (MITP) with the RF drive having 90° phase difference between stages to obtain the frequency quadrupling function [42]. An equivalent effect as the quadrature RF drive to the second stage is obtained with in-phase RF drive by inserting a tunable optical delay line to adjust the relative phase of the sidebands generated by the first stage [43]. By setting the first MZM at the MITP and the second MZM at the maximum transmission point (MATP) or vice-versa frequency sextupling is achieved [44, 46]. By biasing both the MZM at the MATP frequency octo-tupling is achieved with appropriate adjustment of the tunable optical delay line and RF drive level [45-46].

Although a single stage parallel MZM structure has been found in the previous chapter capable of filter-less and dc bias-less octo-tupling without the requirement of precise adjustment of RF drive and/or tunable delays; as far as the authors are aware, an equivalent two stage MZM with series-parallel structure is not known in the prior art. In this chapter, a generalized theory is discussed when two MZM is connected in series with same electrical drive to both of them and in-phase and quadrature electrical drive. Using the general theory, a novel design is proposed for the first time where a Mach-Zehnder interferometer with each arm containing a pair of Mach-Zehnder Modulators in series as a means of optoelectronic frequency octo-tupling multiplication. The optical carrier and all sidebands except those with orders equal to an odd integer multiple of four are naturally suppressed. The circuit requires no electrical or optical filters. There is no requirement to carefully adjust the modulation index to achieve correct operation of the octo-tupler. Moreover the circuit requires 50% of the RF power required by the functionally equivalent single-stage parallel MZM architecture for the same output. If the RF drive is adjusted to suppress the fourth order sidebands, the same configuration can be used for frequency quattuorviginti-tupling.

In this chapter, the circuit architecture is first described and its operation analyzed theoretically using a transfer matrix approach. The theoretical predictions are then validated by the results of computer simulation using the Virtual Photonics Inc. software package. The

simulation results are also presented to illustrate the impact on the circuit performance of the non-idealities encounter in practice such as power splitting imbalance of the optical coupler, phase imbalance and phase errors of the RF signals reaching the modulators. Finally, a comparison is presented with a functionally equivalent single stage GMZI as described in chapter 3.

4.2 Theoretical Analysis

When a MZM is biased at its maximum transmission point, ($v_{DC1} = v_{DC2} = 0$) its amplitude transmission function can be written as:

$$h = \cos(\pi v / v_{\pi}) \tag{4.1}$$

where v_{π} is the half wave voltage of the modulator and v is the applied RF signal. Similarly, when the MZM is biased at minimum transmission point, meaning that the applied DC bias is one half of the half-wave voltage ($v_{DC} = v_{\pi}/2$), the amplitude transmission function is:

$$h = \sin(\pi v / v_{\pi}) \tag{4.2}$$

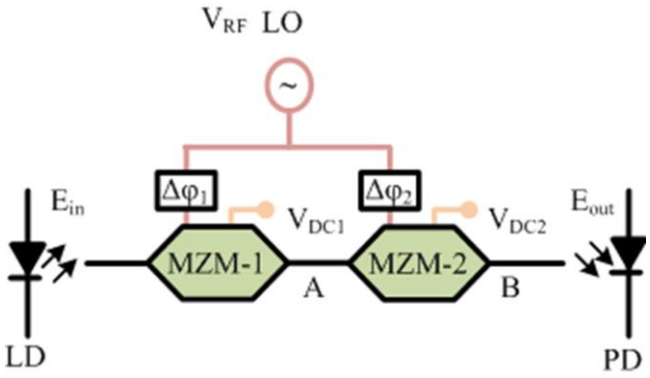

Fig. 4.1. A two-stage cascade MZM. LD, Laser diode; PD, photodiode; V_{RF} LO, Radio frequency local oscillator.

When two such MZM are back to back connected then it is called a two-stage cascade MZM structure. Fig 4.1 shows an example of such architecture. A two-stage cascade of MZM can be biased at one of following options.

i) MATP and MATP
ii) MITP and MITP
iii) MATP and MITP

iv) MITP and MATP

In the following, a through theoretical analysis of the four bias combinations will be discussed for the setup of Fig 4.1.

4.2.1 MATP, MATP

When both the MZM are biased at maximum transmission point, the amplitude transmission function will be,

$$h_{MATP,MATP} = \cos(\pi v_1/v_\pi)\cos(\pi v_2/v_\pi) \quad (4.3)$$

Using trigonometric identities, Equation (4.3) can be written as:

$$h_{MATP,MATP} = \frac{1}{2}\{\cos[\pi(v_1 - v_2)/v_\pi] + \cos[\pi(v_1 + v_2)/v_\pi]\} \quad (4.4)$$

Assume the same RF drive to each stage,

$$v_1 = v_2 = v_{RF}\cos(\omega_{RF}t) \quad (4.5)$$

where v_{RF} is the peak RF amplitude, ω_{RF} is the RF angular frequency, t is time.

Substituting Equation (4.5) into Equation (4.4) and developing,

$$h_{MATP,MATP} = 1/2\,\{1 + cos[\pi v_{RF}/v_\pi \cos(\omega_{RF}t)]\} \quad (4.6)$$

Using the Jacobi-Anger expansion, one may write:

$$\cos[m\cos(\omega_{RF}t \pm \Delta\varphi_P)] = J_0(m) + 2\sum_{n=1}^{\infty}(-1)^n J_{2n}(m)\cos(2n\omega_{RF}t \pm 2n\Delta\varphi_P) \quad (4.7)$$

where, J_n is the Bessel function of the first kind of order n.

Expanding the right hand terms of Equation (4.7) for Equation (4.6), the output signal of the architecture can be represented as:

$$E_{out}(\mathrm{t}) = 1/2\{1 + J_0(\mathrm{m}) + 2\,[J_2(m)\cos(2\omega_{RF}\mathrm{t}) + J_4(\mathrm{m})\cos(4\omega_{RF}\mathrm{t}) + \cdots]\}\,E_{in}(t) \quad (4.8)$$

Where

$$m = \pi v_{RF}/v_\pi \quad (4.9)$$

is the modulation index.

Equation (4.8) shows that all the odd-order harmonics are suppressed while all the even-order harmonics are generated (Fig 4.2). These expressions do not seem particularly useful for frequency multiplication application.

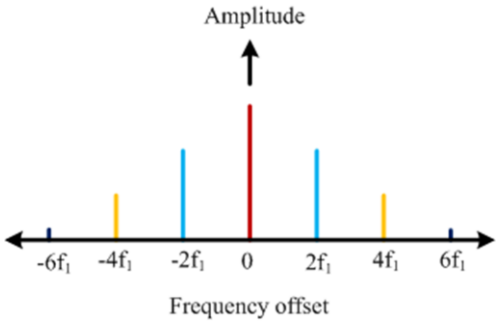

Fig. 4.2. Schematic of the output optical spectrum when two MZM are in cascade (both biased at MATP) with same RF drive; f_1 is the applied RF signal frequency.

If in-phase and quadrature drives are chosen for MZM-1 and MZM-2, then

$$v_1 = v_{RF}\cos(\omega_{RF}t) \tag{4.10}$$

$$v_2 = v_{RF}\sin(\omega_{RF}t) \tag{4.11}$$

Substituting Equation (4.10) & Equation (4.11) into Equation (4.4), gives

$$h_{MATP,MATP} = \frac{1}{2}\{\cos[m\cos(\omega_{RF}t - \pi/4)] + \cos[m\cos(\omega_{RF}t + \pi/4)]\} \tag{4.12}$$

Where,

$$m = \sqrt{2}\pi v_{RF}/v_\pi \tag{4.13}$$

is the modulation index. It can be conclude from Equation (4.9) & Equation (4.13), when both the MZM are biased with in-phase and quadrature drive, the required RF drive is 3 dB less in power than when they are biased with same RF drive to each stage.

Using Jacobi anger expansion, expanding Equation (4.12) and simplifying,

$$E_{out}(\mathrm{t}) = \{J_0 + 2\,[\,J_4(m)\cos(4\omega_{RF}\mathrm{t}) + J_8(\mathrm{m})\cos(8\omega_{RF}\mathrm{t}) + \cdots\,]\}E_{in}(t) \tag{4.14}$$

It shows that optical harmonics other than integer multiple of four are totally suppressed (as shown in Figure 4.3). Hence only orders equal to $4l$ with l an integer are unsuppressed. The

most significant orders are the carrier and the 4th orders side-bands, adjusting the drive to suppress the carrier, yields a frequency octo-tupler.

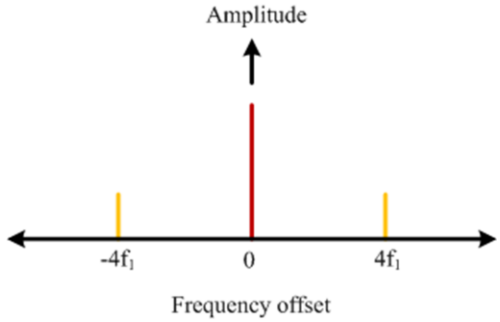

Fig. 4.3. Schematic of the output optical spectrum when two MZM are in cascade (both biased at MATP) with in-phase and quadrature RF drive.

4.2.2 MITP, MITP

When both the MZM are biased at minimum transmission point, the amplitude transmission function will be,

$$h_{MITP,MITP} = \sin(\pi v_1/v_\pi)\sin(\pi v_2/v_\pi) \quad (4.15)$$

Using trigonometric identities, Equation (4.15) can be written as:

$$h_{MITP,MITP} = \frac{1}{2}\{\cos[\pi(v_1 - v_2)/v_\pi] - \cos[\pi(v_1 + v_2)/v_\pi]\} \quad (4.16)$$

Applying same RF drive to the Equation (4.16) and developing,

$$h_{MITP,MITP} = 1/2\,\{1 - cos[\pi v_{RF}/v_\pi \cos(\omega_{RF}t)]\} \quad (4.17)$$

Expanding the right hand terms of Equation (4.17) using Jacobi Anger expression, the output signal of the architecture can be represented as:

$$E_{out}(\mathrm{t}) = 1/2\{1 - J_0(\mathrm{m}) + 2\,[J_2(m)\cos(2\omega_{RF}\mathrm{t}) + J_4(\mathrm{m})\cos(4\omega_{RF}\mathrm{t}) + \cdots]\}\,E_{in}(t) \quad (4.18)$$

Equation (4.18) shows that all the odd-order harmonics are suppressed while all the even-order harmonics are unsuppressed (Figure 4.4). As same for the above combination (MATP, MATP) the expression do not seem particularly useful for frequency multiplication application.

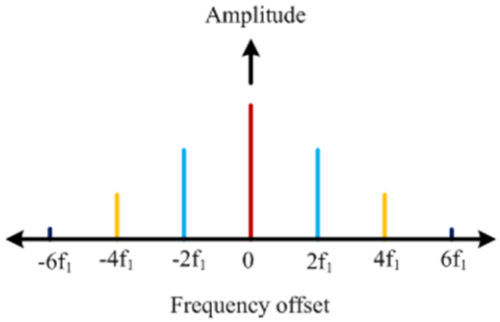

Fig. 4.4. Schematic of the output optical spectrum when two MZM are in cascade (both biased at MITP) with same RF drive.

If in-phase and quadrature drives are chosen for MZM-1 and MZM-2, then Equation (4.16) can be written as:

$$h = \frac{1}{2}\{\cos[m\cos(\omega_{RF}t - \pi/4)] - \cos[m\cos(\omega_{RF}t + \pi/4)]\} \quad (4.19)$$

Using Jacobi Anger expansion, expanding Equation (4.19) and simplifying,

$$E_{out}(\mathrm{t}) = \{2\mathrm{i}\,[\,J_2(m)\cos(2\omega_{RF}\mathrm{t}) + J_6(\mathrm{m})\cos(6\omega_{RF}\mathrm{t}) + \cdots]\}E_{in}(t) \quad (4.20)$$

It shows that all the optical harmonics are suppressed other than $2l + 2$, where l is an even integer (Figure 4.5). The most significant sidebands are therefore the 2nd order sidebands, yielding frequency four multiplication when the signal is passed through a square-law photo-detector. If the drive (modulation index) is adjusted to suppress these sidebands, the next most significant sidebands are the 6th order, yielding a frequency 12 multiplier.

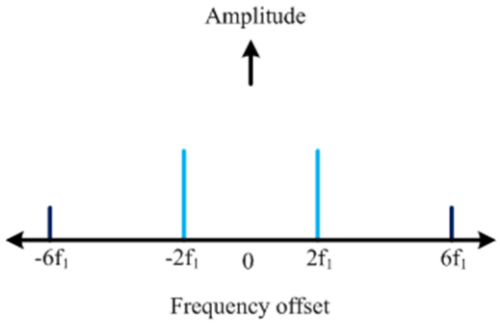

Fig. 4.5. Schematic of the output optical spectrum when two MZM are in cascade (both biased at MITP) with in-phase and quadrature RF drive.

4.2.3 MATP, MITP

When the first MZM is biased at maximum transmission point and second stage MZM is biased at minimum transmission point, the amplitude transmission function will be,

$$h_{MATP,MITP} = \cos(\pi v_1/v_\pi)\sin(\pi v_2/v_\pi) \tag{4.21}$$

Using trigonometric identities, Equation (4.21) can be written as:

$$h_{MATP,MITP} = \frac{1}{2}\{-\sin[\pi(v_1 - v_2)/v_\pi] + \sin[\pi(v_1 + v_2)/v_\pi]\} \tag{4.22}$$

Assume the same RF drive to each stage and doing further simplification Equation (4.22) gives us:

$$h_{MATP,MITP} = 1/2\,\{sin[\pi v_{RF}/v_\pi \cos(\omega_{RF}t)]\} \tag{4.23}$$

Using the Jacobi-Anger expansion, one may write:

$$\sin[m\cos(\omega_{RF}t \pm \Delta\varphi_P)] = -2\sum_{n=1}^{\infty}(-1)^n J_{2n-1}(m)\cos\{(2n-1)\omega_{RF}t \pm (2n-1)\Delta\varphi_P\} \tag{4.24}$$

Expanding the right hand terms of Equation (4.23) using Equation (4.24), the output signal of the architecture can be represented as:

$$E_{out}(\mathrm{t}) = 1/2\{2\,[J_1(m)\cos(\omega_{RF}\mathrm{t}) - J_3(\mathrm{m})\cos(3\omega_{RF}\mathrm{t}) + J_5(m)\cos(5\omega_{RF}\mathrm{t}) \ldots]\}\,E_{in}(t) \tag{4.25}$$

Where, $m = \pi v_{RF}/v_\pi$ (4.26)

is the modulation index.

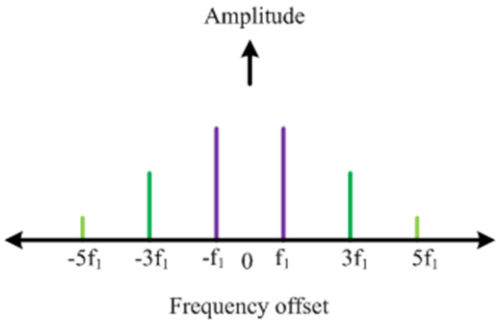

Fig. 4.6. Schematic of the output optical spectrum when two MZM are in cascade (1st MZM biased at MATP & later is biased at MITP) with same RF drive.

Equation (4.25) shows that all the even-order harmonics are suppressed (Fig 4.6)

If in-phase and quadrature drives are chosen for MZM-1 and MZM-2, then

$$h_{MATP,MITP} = \frac{1}{2}\{-\sin[m\cos(\omega_{RF}t - \pi/4)] + \sin[m\cos(\omega_{RF}t + \pi/4)]\} \quad (4.27)$$

Where,

$$m = \sqrt{2}\pi v_{RF}/v_{\pi} \quad (4.28)$$

is the modulation index.

Applying the Jacobi Anger expansion Equation (4.27) can be written as,

$$E_{out}(t) = [\sum_{n=1}^{\infty}(-1)^n J_{2n-1}(m)\cos\{(2n-1)\omega_{RF}t\} - \sum_{n=1}^{\infty}(-1)^n J_{2n-1}(m)\cos\{(2n-1)\omega_{RF}t\}]E_{in}(t) \quad (4.29)$$

It shows that all the even order optical harmonics are totally suppressed (as shown in Fig 4.7).

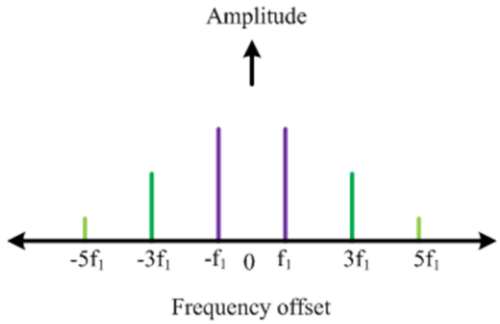

Fig. 4.7. Schematic of the output optical spectrum when two MZM are in cascade (1st MZM biased at MATP & later is biased at MITP) with in-phase and quadrature RF drive.

4.2.4 MITP, MATP

When both the first MZM is biased at minimum transmission point and the second stage MZM is biased at maximum transmission point, the amplitude transmission function will be,

$$h_{MITP,MATP} = \cos(\pi v_1/v_{\pi})\sin(\pi v_2/v_{\pi}) \quad (4.30)$$

Using trigonometric identities, Equation (4.30) can be written as:

$$h_{MITP,MATP} = \frac{1}{2}\{\sin[\pi(v_1 - v_2)/v_\pi] + \sin[\pi(v_1 + v_2)/v_\pi]\} \quad (4.31)$$

Assume the same RF drive to each stage and doing further simplification Equation (4.31) gives us:

$$h_{MITP,MATP} = 1/2\,\{sin[\pi v_{RF}/v_\pi \cos(\omega_{RF}t)]\} \quad (4.32)$$

Expanding the right hand terms of Equation (4.32) using Equation (4.24), the output signal of the architecture can be represented as:

$$E_{out}(\mathrm{t}) = 1/2\{2\,[J_1(m)\cos(\omega_{RF}\mathrm{t}) - J_3(\mathrm{m})\cos(3\omega_{RF}\mathrm{t}) + J_5(m)\cos(5\omega_{RF}\mathrm{t}) \ldots]\}\,E_{in}(t) \quad (4.33)$$

Where

$$m = \pi v_{RF}/v_\pi \quad (4.34)$$

is the modulation index.

Equation (4.33) shows that all the even-order harmonics are suppressed (Figure 4.8).

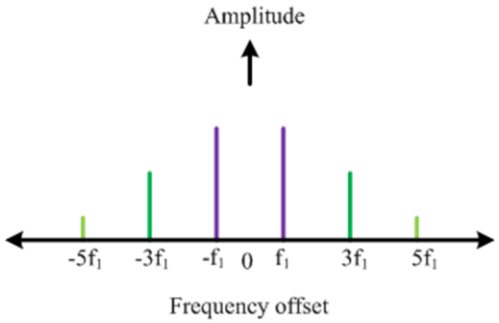

Fig. 4.8. Schematic of the output optical spectrum when two MZM are in cascade (1st MZM biased at MITP & later is biased at MATP) with same RF drive.

If in-phase and quadrature drives are chosen for MZM-1 and MZM-2, then

$$h_{MITP,MATP} = \frac{1}{2}\{\sin[m\cos(\omega_{RF}t - \pi/4)] + \sin[m\cos(\omega_{RF}t + \pi/4)]\} \quad (4.35)$$

Where,

$$m = \sqrt{2}\pi v_{RF}/v_\pi \quad (4.36)$$

is the modulation index.

Applying the Jacobi Anger expansion Equation (4.35) can be written as,

$$E_{out}(t) = [-\sum_{n=1}^{\infty}(-1)^n J_{2n-1}(m)\cos\{(2n-1)\omega_{RF}t\} - \sum_{n=1}^{\infty}(-1)^n J_{2n-1}(m)\cos\{(2n-1)\omega_{RF}t\}]E_{in}(t) \quad (4.37)$$

It shows that all the even order optical harmonics are totally suppressed (as shown in Fig 4.9).

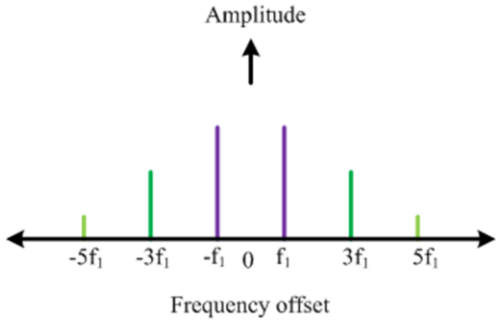

Fig. 4.9. Schematic of the output optical spectrum when two MZM are in cascade (1st MZM biased at MATP & later is biased at MITP) with in-phase and quadrature RF drive.

It can be observed from the above mentioned analysis that a two stage cascade MZM structure is useful for frequency multiplication when in-phase and quadrature drive is used along with both the MZM are biased at maximum transmission point or minimum transmission point. The frequency multiplication can be achieved from the analysis is depend upon the careful adjustment of modulation index to suppress the unwanted harmonics. Using this knowledge, a more useful circuit structure can be proposed that can generate frequency-8 multiplication, where the performance of the architecture is not limited by careful adjustment of the modulation index. If modulation index can be adjusted, the proposed design can be used to generate frequency 24-tupling.

The newly proposed circuit architecture, shown in Fig 4.10, is formed by an outer Mach-Zehnder interferometer (MZI) biased at its MITP with each of its two arms containing a pair of MZMs in series; each biased at its MATP. The first and second stages are driven in quadrature by the RF signal. Each arm generates optical sidebands with orders equal to an integer multiple of four. When combined by the outer MZI, the orders equal to an even

integer multiple of four are suppressed; only orders equal to an odd integer multiple of four ($\pm 4, \pm 12, \pm 20 \ldots$) are unsuppressed. On photo-detection, the optical output is converted to an electrical current with the strongest oscillatory component at a frequency equal to eight-times the base RF frequency. If the RF drive level is adjusted to suppress the fourth-order optical sidebands, the strongest oscillatory component of the current has a frequency equal to twenty-four times the base RF frequency**.**

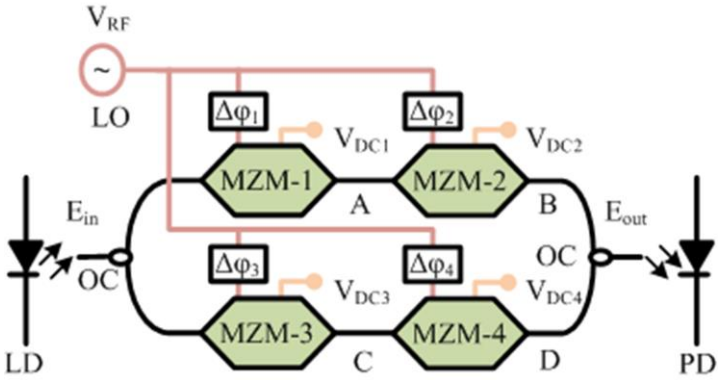

Fig. 4.20. Schematic diagram of the frequency octo-tupler circuit using Mach-Zehnder modulator in cascade; LD, Laser diode; OC, Optical coupler; RF, Radio frequency; LO, RF Local oscillator; PD, Photodiode.

When a two-stage cascade of MZMs is biased at MATP (according to the Fig 4.10, when ($v_{DC1} = v_{DC2} = v_{DC3} = v_{DC4} = 0$), the amplitude transmission function can be written from Equation (4.3)

$$h_{MATP,MATP} = \cos(\pi v_a / v_\pi) \cos(\pi v_b / v_\pi) \tag{4.38}$$

Hence, the transmission functions of the two arms (MZM-1& MZM-2; MZM-3 &MZM-4) are:

$$h_{12} = \cos(\pi v_1 / v_\pi) \cos(\pi v_2 / v_\pi) \tag{4.39}$$

$$h_{34} = \cos(\pi v_3 / v_\pi) \cos(\pi v_4 / v_\pi) \tag{4.40}$$

Now the output of the whole circuit can be written:

$$\begin{bmatrix} E_{out} \\ 0 \end{bmatrix} = H \begin{bmatrix} \mathrm{h}_{12} & 0 \\ 0 & \mathrm{h}_{34} \end{bmatrix} H \begin{bmatrix} E_{in} \\ 0 \end{bmatrix} \tag{4.41}$$

Where E_{in}, E_{out} are the overall input and output optical field amplitudes respectively and:

$$H = \begin{bmatrix} \sqrt{\alpha} & -i\sqrt{1-\alpha} \\ -i\sqrt{1-\alpha} & \sqrt{\alpha} \end{bmatrix} \tag{4.42}$$

is the transfer matrix of the optical coupler and α is the coupling factor. For the ideal case $\alpha = 1/2$. Here the optical coupler is assumed to be a 2×2 Multimode Interference Coupler or Directional Coupler rather than a y-branch coupler. This ensures that the outer MZI is naturally biased at its MITP. Developing Equation (4.41), the output in the ideal case yields:

$$E_{out} = \frac{1}{2}\,(h_{12} - h_{34})E_{in} \tag{4.43}$$

With the aid of trigonometric identities, Equation (4.39) & (40) can be re-expressed as:

$$h_{12} = \frac{1}{2}\{\cos[\pi(v_1 - v_2)/v_\pi] + \cos[\,\pi(v_1 + v_2)/v_\pi]\} \tag{4.44}$$

$$h_{34} = \frac{1}{2}\{\cos[\,\pi(v_3 - v_4)/v_\pi] + \cos[\,\pi(v_3 + v_4)/v_\pi]\} \tag{4.45}$$

Assume the RF drive is given by $v_P = v_{RF}\cos(\omega_{RF}t + \Delta\varphi_P)$, where v_{RF} is the peak RF amplitude, ω_{RF} is the RF angular frequency, t is time and $\Delta\varphi_P$ is the phase of the p^{th} RF drive. Setting the RF phase shifts to $\Delta\varphi_1 = 0$, $\Delta\varphi_2 = \pi/2$, $\Delta\varphi_3 = \pi/4$, and $\Delta\varphi_4 = 3\,\pi/4$ and developing Equation (4.44) & (45):

$$h_{12} = \frac{1}{2}\{\cos[m\cos(\omega_{RF}t - \pi/4)] + \cos[m\cos(\omega_{RF}t + \pi/4)]\} \tag{4.46}$$

$$h_{34} = \frac{1}{2}\{\cos[m\cos(\omega_{RF}t)] + \cos[m\cos(\omega_{RF}t + \pi/2)]\} \tag{4.47}$$

where:

$$m = \sqrt{2}\pi v_{RF}/v_\pi \tag{4.48}$$

is the modulation index. Which yields,

$$v_{RF} = mv_\pi/\pi\sqrt{2} = v_{SS}/\sqrt{2} \tag{4.49}$$

where V_{SS} is the RF voltage required for the functionally equivalent single stage parallel structure described in previous chapter. Equation (4.49) show that the required RF amplitude for a two stage series-parallel structure 3 dB less than of the functionally equivalent single stage parallel structure.

Using the Jacobi-Anger expansion, one may write:

$$\cos[m\cos(\omega_{RF}t + \Delta\varphi_P)] = J_0(m) + 2\sum_{n=1}^{\infty}(-1)^n J_{2n}(m)\cos(2n\omega_{RF}t + 2n\Delta\varphi_P) \quad (4.50)$$

where, J_n is the Bessel function of the first kind of order n.

Expanding the right-hand terms of Equation (4.50) for the specified phase shifts $\Delta\varphi_P$, substituting them into Equation (4.43) and eliminating the common terms, the output signal can be represented as

$$E_{out} = 2\,[\,J_4(m)\cos(4\omega_{RF}\mathrm{t}) + J_{12}(\mathrm{m})\cos(12\omega_{RF}\mathrm{t}) + \cdots]E_{in} \quad (4.51)$$

It can be seen from the process leading to Equation (4.43), that all the orders are suppressed except those for which $n = 4l$, where l is an odd integer. Furthermore, the term $J_{12}(\mathrm{m})$ is negligible when the modulation index $m \leq 7.30$, and the circuit performs as frequency octo-tupler after passing the output onto a photodiode. On the other hand, by adjusting the modulation index ($m = 11.06$ or 14.37) to set $J_4(m) = 0$, the same architecture can be used for quattuorviginti-tupling (24-tupling).

4.3 Simulation Result

The operation of the proposed circuit was verified by computer simulations using the Virtual Photonic Inc. (VPI) software package. A continuous-wave DFB laser diode operating at a vacuum wavelength of 1550 nm with a line-width of 200 kHz and an emission power of 10 mW is used as the optical input. The circuit can be operated over a wide range of modulation index (~2 to ~7.30) as its correct function is not restricted to a particular electrical drive level. In order to maximize the output electrical power of the octo-tupled function, a modulation index of $m = 5.28$ is used in this simulation, which implies a peak RF drive voltage of $v_{RF} = 1.18\,v_\pi$, ~30% less (50% in power) than the voltage required ($v_{RF} = 1.68\,v_\pi$) for same modulation index that uses the single-stage parallel MZM configuration in the previous chapter. The half-wave voltage, v_π of the phase modulators is set to 5 V as representative of commercially available $LiNbO_3$ modulators (A differentially driven MZM formed from a pair of these phase modulators has a switching voltage of half this value.). The RF drive frequency is set to 7.5 GHz. In the ideal case, the extinction ratio is infinite (80 dB is set in VPI) for all the MZMs; the optical coupler/splitter is perfectly balanced (50%) with ideal $0, \pi/2$ relative phases between its ports; and the phase shifts applied to the RF drive are exactly as specified; a frequency octo-tupling function is achieved. As shown in

Figure 4.11 (a) fourth harmonics at ±30 GHz (4×7.5 GHz) with 70 dB suppression from the unwanted twelfth (±90 GHz) harmonics is obtained. After passing through a photo-detector, a pristine frequency component at 60 GHz is obtained without any unwanted harmonics as shown in Fig 4.11 (b).

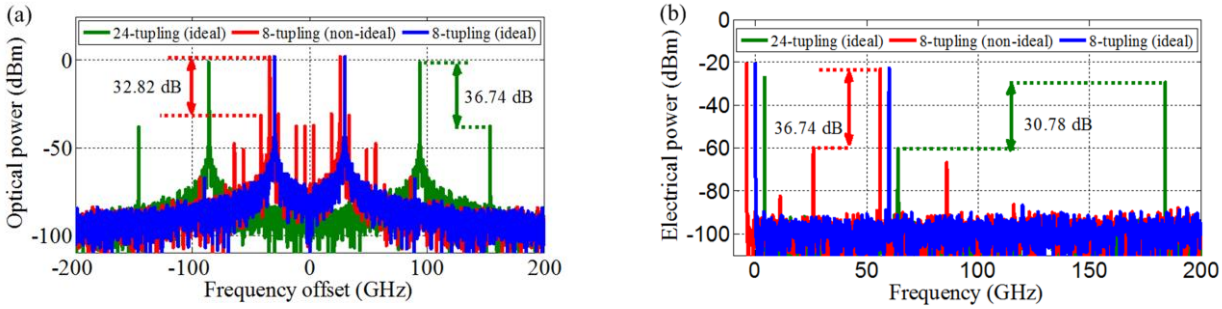

Fig. 4.11. (a) Optical spectrum of the output signal. (b) Electrical spectrum of the signal after photo-detection. For visualization, plots for 8-tupling (non-ideal) and 24-tupling (ideal) are frequency shifted by ∓4 GHz.

Fig 4.12(a) shows the relationship between the peak electrical power of the harmonics of interest ($8f_{RF}$) and unwanted harmonics ($2f_{RF,}$ $4f_{RF,}$ $6f_{RF}$) for a wide range of modulation index with 30 dB extinction ratio of the MZMs. It shows that the operation of the proposed circuit does not depend on the careful adjustment of the RF drive to the Mach-Zehnder modulators, rather it can be operated any point between $2 \leq m \leq 7.30$. Simulations accounting for component impairments found in practice, such as the finite extinction ratio of the MZMs and imbalances in the splitting ratio of the optical coupler, have been conducted to assess their impact on the 8-fold frequency multiplication circuit performance under non-ideal conditions. Figure 4.12(b) shows the relationship between the extinction ratio of the MZM and the numerically calculated electrical harmonic distortion suppression ratio (EHDSR) for specific power imbalances (2% & 5%) between the ports of the input optical coupler. Simulation result shows, for a power imbalance of 5% (55% & 45%) between the ports of the input optical coupler, the EHDSR is over 36 dB regardless the value of extinction ratio ranging from 25 dB to 80 dB and over 44 dB when the optical coupling factor is 48% (or 2% power imbalance). As an example, the non-ideal 8-tupling presented in Fig 4.11(a) & (b) for 5% power imbalances with 30 dB extinction ratio. Hence the appearance of unwanted harmonics to a large extent depends on the power splitting ratio of

the input coupler. Nevertheless, the EHDSR is still above 36 dB for 5% imbalances in splitting ratio with an extinction ratio minimum of 25 dB.

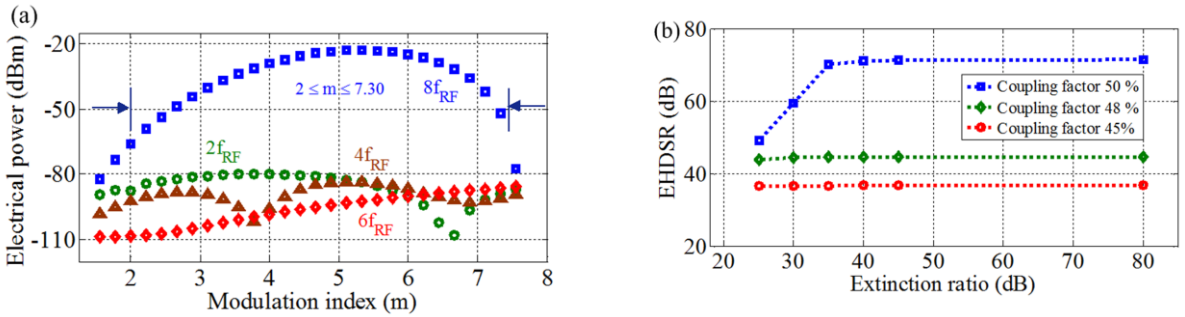

Fig.4.12. (a) Electrical peak power of the harmonics of interest and unwanted harmonics (b) EHDSR for a wide range of extinction ratio with power imbalances (2% & 5%) at the input optical coupler.

It is found in the previous chapter that the phase errors of the drive signal at the modulators are the critical part of the design; hence the waveguides that connected between the RF drive and MZM must be taken into account. Fig 4.13(a) shows the phase errors of applied RF signals from 0° (ideal case) to 5° both in a differential MZM (i.e., (0 & π)$\pm$5° in MZM-1) and a single phase modulators (i.e., 0$\pm$5° in the top phase modulator of MZM-1). It shows that, for a 5° phase error in the drive signal, the parallel architecture has an EHDSR of 18 dB compared to 14 dB for the cascade series-parallel architecture. All MZMs have an extinction ratio of 30 dB. Figure 4.13(b) shows the EHDSR for the power imbalances and phase errors between the output ports of the input optical coupler. The phase imbalances between the ports of the coupler has very little impact on the performance of the 8-tupling operation as the EHDRS is still 50 dB (the single stage parallel circuit has a 4 dB advantage) for 5° error. The EHDSR is over 36 dB for 5% imbalances for the configurations.

Furthermore, both circuits (cascade and equivalent single stage) have 4 MZMs, and 2 direction couplers (optical bias using an optical delay line can be avoided by replacing the input and output Y-splitter and combiner by direction couplers). In addition to that, the single stage architecture requires an additional two Y-splitters and Y-combiners which contribute an excess optical loss relative to the cascade architecture.

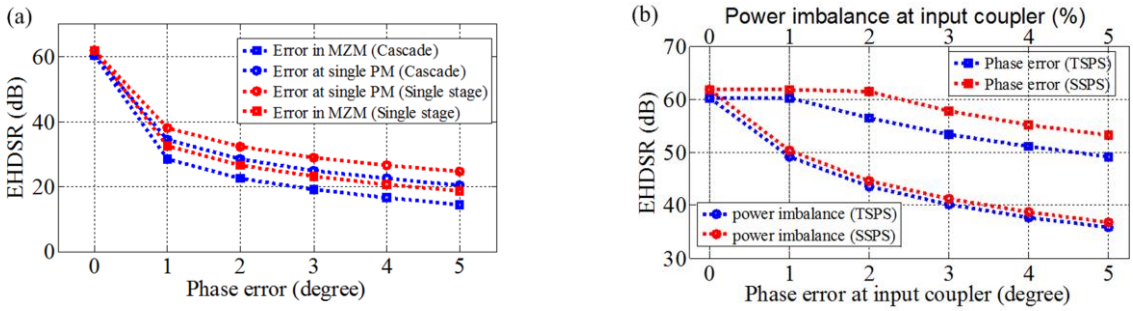

Fig. 4.13. Comparison between proposed cascade structure with functionally equivalent single stage structure. (a) EHDSR for phase errors between MZM and at single PM. (b) EHDSR for power imbalances and phase error between the output ports of the input coupler.

As depicted in Figure 4.2, by setting the modulation index to $m \approx 14.37$ with all other conditions remaining ideal (perfect split and phase relation among the ports of optical coupler and perfect phase relationships among the RF drive), frequency quattourviginti-tupling of the input RF signal is achieved. As shown, the 20^{th} harmonics (± 150 GHz) are suppressed by 36.74 dB optical relative to the 12^{th} harmonics at ± 90 GHz, while the quattourviginti-tupled frequency (180 GHz) has an EHDSR of about 31 dB over the frequency components present at 60 GHz.

4.4 Summary & Discussion

In summary, a basic theory based on two-stage cascade MZM structure is proposed. It shows that, when both the MZMs are biased at MATP or MITP with in-phase and quadrature drive signal to them is desirable for frequency multiplication application. Furthermore, using the basic theoretical concept, a novel photonic circuit architecture featuring a two-stage cascade MZM structure has been proposed for the first time for implementing frequency octo-tupling and quattuorviginti-tupling (24-tupling) and its operation analysed. The predictions of the theoretical analysis have been verified by computer simulations. The operation of the octo-tupler circuit is not restricted by any requirement to set the amplitude of the drive signal to a precise level. Moreover, in principal the circuit requires no DC bias and optical filtering to suppress the unwanted harmonics. The analysis and simulations prove that, the two-stage cascade MZM configuration is advantageous compared to the single-stage parallel MZM configuration with equivalent function, as it requires 3 dB less power in RF drive for the

same output when the applied RF signals reaching to the MZM with perfect phase relations. However, the single-stage parallel MZM configuration has 4 dB advantages in Electrical SHSR compared to the two-stage serial-parallel MZM structure when imperfect scenarios such as phase errors of the RF signals are considered. Nevertheless, when the applied RF signal has no phase errors, over 30 dB harmonic suppression is obtained in both optical and electrical domain when the extinction ratio of MZM is at least 25 dB and there is less than 5% power imbalance between the ports of the input coupler is applied. Furthermore, the proposed design can be implemented using mature $LiNbO_3$ technology.

Chapter 5. High order USB and LSB Separation for Remote Heterodyning

5.1. Introduction

A major pre-requisite for the widespread deployment of high-capacity digital coherent radio-over-fibre (RoF) systems is the effective generation and transmission of millimeter wave (mm-wave) carriers over fibre at the down link (central office to base station/remote unit). The fundamental principle of microwave photonics is the heterodyne beating of two optical carriers separated in frequency at a high speed photo-detector which provides a conceptually simple means of generating widely-tunable mm-wave carriers. The spectral purity of the mm-wave carrier is related to the phase correlation of the two optical carriers. The generation of a pair of optical carriers separated in frequency by the external modulation of lasers is superior to other technique such as optical-injection locking between master-slave lasers and optical-electrical phase loops because it offers highly stable and highly phase correlated carriers with system simplicity. The phase of the optical carrier is modulated by the RF frequency to create a multitude of phase correlated spectral lines indexed by the frequency of the RF harmonics ($\pm 1 f_{RF}, \pm 2 f_{RF}, \cdots$) relative to the optical carrier, where f_{RF} is the applied RF frequency. Exploiting this phase correlation the modulated optical output of multiple phase modulators driven from the same optical and electrical sources but with carefully chosen electrical and optical relative phase shifts may be combined so that only two optical lines with significant amplitude separated by a desired multiple of the RF frequency may be generated.

A significant number of architecture based on the external modulation has been proposed [29-47] to achieve different order frequency multiplication. The majority of these proposals [29-41] employ a single stage generalized Mach-Zehnder Interferometer (GMZI) architecture, where N parallel phase modulators are connected between a $1:N$ splitter and $N:1$ coupler. For even N, the individual phase modulators may be re-ordered to form a pair of differentially driven Mach-Zehnder Modulator (MZM). A much fewer number of proposals have considered a two-stage architecture where the basic element, i.e., MZMs are connected in series [42-46] or both in series and parallel [47]. The first experimental demonstration of a frequency doubler was reported [29] more than two decades ago. Since

then, different high order multiplication factors have been reported theoretically and/or experimentally; for example, circuit designs for frequency quadrupling [30-32, 42-43], sextupling [33, 44, 47], octo-tupling [35-38, 45-46] and by higher factors [39-41] have been reported. Common demerits of the proposed circuits are the use of static DC bias; the use optical filtering; and the adjustment of the electrical drive level to suppress unwanted harmonics. A DC bias-less, filter-less frequency octo-tupler that can operate for a wide range of modulation index reported in previous two chapters (Chapter 3 & 4), represents significant progress in addressing these demerits.

A common feature of all the reported circuit designs is that the pair of high-order harmonics separated by the desired RF carrier frequency (± 4 for frequency octo-tupling) is emitted from the same output port. The pair of carriers must therefore be separated as the data to be transported must modulate only one. This can be done by using frequency selective components such as arrayed waveguide gratings (AWGs). But this severely restricts the tuning range to the bandwidth of the frequency selective components and introduces frequency alignment issues that require temperature stabilisation. . Hence, there is a requirement for a circuit that can generate two high order harmonics that are emitted from different output ports ($+4$ from one port and -4 from another port). This carrier separation eliminates the need for thermal stabilisation.

In this work, the design of a photonic integrated circuit is presented, that can generate two high order harmonics from the two output ports ($+2$ from the upper output port and -2 from the lower output port). A complete (down-link) simulation of the digital coherent RoF system is presented as an application of the proposed circuit.

5.2. Principle of operation

The PIC may employ either a single stage parallel MZM architecture or an equivalent two stage series-parallel MZM architecture. Both the architectures are discussed in this section.

The single stage parallel MZM architecture, shown in Fig. 1, forms an outer Mach-Zehnder interferometer (MZI) that is biased by a static phase shift at its Quadrature Transmission Point (QTP) Each of the two arms of the outer MZI form an inner MZI that is biased at their Minimum Transmission Point (MITP). Each arm of the inner MZIs contains a MZM that is biased at its Maximum Transmission Point (MATP). Equivalently, the circuit may be

considered as consisting of an outer MZI biased at its QTP with each of its two arms containing a Dual-Parallel Mach-Zehnder Modulator (DP-MZM) with its inner MZI biased at their MITP and its MZM biased at their MATP The two MZM of the DP-MZM are driven by in-phase and quadrature RF signals. Hence, each DP-MZM generates optical sidebands with orders equal to $2l$ where l is an odd integer. When combined by the outer MZI, each pair of unsuppressed side bands with same magnitude orders but alternative sign are separated at the two output ports rather than exiting as a pair from the same output port. Specifically in this case the +2,-6, +10... orders exit the upper port and the -2,+6,-10…. orders exit from lower port. If the RF drive level is adjusted to suppress the second-order optical sidebands, the strongest side-bands will correspond to the 6th harmonic of the electrical drive signal.

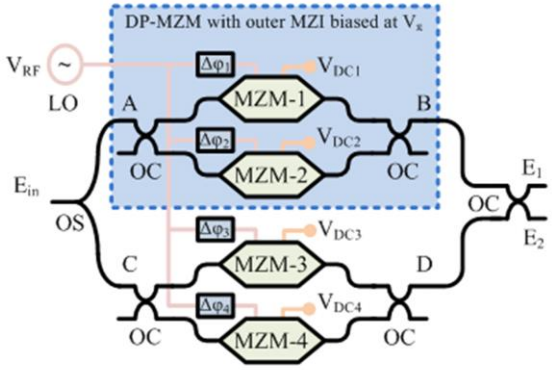

Fig. 5.1. Schematic diagram of the hgh-order single sideband separation circuit using four Mach-Zehnder modulators in parallel; OC, Optical coupler; OS, Optical splitter; RF, Radio frequency; LO, RF Local oscillator.

When a MZM is biased at its maximum transmission point, its amplitude transmission function can be written as:

$$h = \cos(\pi v / v_\pi) \tag{5.1}$$

where v_π is the half wave voltage of the phase modulators that comprise the MZM and v is the applied RF signal.

Hence the transmission from node A to node B of the circuit is given by:

$$B = [1 \quad 0] H \begin{bmatrix} h_1 & 0 \\ 0 & h_2 \end{bmatrix} H \begin{bmatrix} 1 \\ 0 \end{bmatrix} A \tag{5.2}$$

Where, in a slight abuse of notation, the optical amplitude at a node has been denoted by the same symbol used to label the node; and,

$$H = \begin{bmatrix} \sqrt{\alpha} & -i\sqrt{1-\alpha} \\ -i\sqrt{1-\alpha} & \sqrt{\alpha} \end{bmatrix} = \frac{1}{\sqrt{2}} \begin{bmatrix} 1 & -i \\ -i & 1 \end{bmatrix} \tag{5.3}$$

is the transfer matrix of the optical coupler and α is the coupling factor. For the ideal case $\alpha = 1/2$. Here the optical coupler is assumed to be a 2×2 Multimode Interference Coupler or Directional Coupler rather than a y-branch coupler. This ensures that the MZI within the DP-MZM is naturally biased at its MITP.

Developing Eq. (5.2) in the ideal case, the output is given by:

$$B = \frac{1}{2}\,(h_1 - h_2)A \tag{5.4}$$

Similarly:

$$D = \frac{1}{2}\,(h_3 - h_4)C \tag{5.5}$$

The overall output of the whole circuit is:

$$\begin{bmatrix} E_1 \\ E_2 \end{bmatrix} = \frac{1}{2} \begin{bmatrix} 1 & -i \\ -i & 1 \end{bmatrix} \begin{bmatrix} B & 0 \\ 0 & D \end{bmatrix} \begin{bmatrix} 1 \\ 1 \end{bmatrix} [E_{in}] \tag{5.6}$$

which yields:

$$E_1 = \frac{1}{2} E_{in}[B - iD] \tag{5.7}$$

$$E_2 = \frac{1}{2} E_{in}[-iB + D] \tag{5.8}$$

and hence:

$$E_2 = -iE_1^* \tag{5.9}$$

Now substituting the values of B and D given by Eq (5.4) and Eq. (5.5) into Eq. (5.7)

$$E_1 = \frac{1}{4} E_{in}[(h_1 - h_2) - i(h_3 - h_4)] \tag{5.10}$$

$$E_1 = \frac{1}{4} E_{in}[\{cos(\pi v_1/v_\pi) - cos(\pi v_2/v_\pi)\} - i\{cos(\pi v_3/v_\pi) - cos(\pi v_4/v_\pi)\}] \tag{5.11}$$

Let the RF drive be given by $v_P = v_{RF}\cos(\omega_{RF}t + \Delta\varphi_P)$, where v_{RF} is the peak RF amplitude, ω_{RF} is the RF angular frequency, t is time and $\Delta\varphi_P$ is the phase of the RF drive

to the p^{th} MZM. Setting the RF phase shifts to $\Delta\varphi_1 = 0$, $\Delta\varphi_2 = \pi/2$, $\Delta\varphi_3 = \pi/4$, and $\Delta\varphi_4 = 3\,\pi/4$ and developing Eq. (5.11) with the aid of the Jacobi-Anger expansion.

$$\cos(z\cos(\theta)) = J_0(z) + 2\sum_{l=1}^{\infty}(-1)^l J_{2l}(z)\cos(2l\theta) \tag{5.12}$$

$$\cos\left(z\cos\left(\theta+\frac{\pi}{2}\right)\right) = J_0(z) + 2\sum_{l=1}^{\infty}(-1)^l J_{2l}(z)\cos(2l\theta + l\pi) =$$

$$J_0(z) + 2\sum_{l=1}^{\infty} J_{2l}(z)\cos(2l\theta) \tag{5.13}$$

$$\cos(z\cos(\theta)) - \cos\left(z\cos\left(\theta+\frac{\pi}{2}\right)\right) = 4\sum_{l\ odd} J_{2l}(z)\cos(2l\theta) \tag{5.14}$$

$$\cos\left(z\cos\left(\theta+\frac{\pi}{4}\right)\right) - \cos\left(z\cos\left(\theta+\frac{\pi}{4}+\frac{\pi}{2}\right)\right) =$$
$$4\sum_{l\ odd} J_{2l}(z)\cos\left(2l\theta + l\frac{\pi}{2}\right) = -4\sum_{l=2k+1}(-1)^k J_{2l}(z)\sin(2l\theta) \tag{5.15}$$

$$\frac{1}{4}\left[\cos(z\cos(\theta)) - \cos\left(z\cos\left(\theta+\frac{\pi}{2}\right)\right)\right] - i\frac{1}{4}\left[\cos\left(z\cos\left(\theta+\frac{\pi}{4}\right)\right) - \cos\left(z\cos\left(\theta+\frac{\pi}{4}+\frac{\pi}{2}\right)\right)\right]$$
$$= \sum_{l=2k+1} J_{2l}(z)\exp((-1)^k 2l\theta) \tag{5.16}$$

and hence:

$$E_1 = [J_2(m)\exp(\mathrm{i}2\omega_{RF}\mathrm{t}) + J_6(\mathrm{m})\exp(-\mathrm{i}6\omega_{RF}\mathrm{t}) + J_{10}(m)\exp(\mathrm{i}10\omega_{RF}\mathrm{t})\ldots]E_{in} \tag{5.17}$$

$$E_2 = -i[J_2(m)\exp(-\mathrm{i}2\omega_{RF}\mathrm{t}) + J_6(\mathrm{m})\exp(\mathrm{i}6\omega_{RF}\mathrm{t}) + J_{10}(m)\exp(-\mathrm{i}10\omega_{RF}\mathrm{t})\ldots]E_{in} \tag{5.18}$$

where, J_n is the Bessel function of the first kind of order n and

$$m = \pi v_{RF}/v_\pi \tag{5.19}$$

is the modulation index.

It can be seen from the process leading to Eq. (5.17) & (5.18), that all the orders are suppressed except those for which $n = \pm(-1)^k 2(2k+1)$where k is a non-negative integer and the alternative sign is chosen as positive for the upper port and negative for the lower port.

The two-stage series parallel MZM architecture shown in Fig. 2. is forms an outer Mach-Zehnder interferometer (MZI) biased at its QTP. Each of its two arms contains a pair of MZMs in series; each biased at its MITP. The first and second stages are driven in quadrature by the RF signal. Each arm generates optical sidebands with orders equal to $2l$ with l is an odd integer. When combined by the outer MZI, each pair of unsuppressed sidebands with same magnitude orders but alternative sign are separated at the two output

ports rather than exiting as a pair from the same output port. Specifically, in this case, the +2 ,-6,+10...orders exit from upper port and the -2,+6,-10…. Orders exit from lower port. If the RF drive level is adjusted to suppress the second-order optical sidebands, the strongest side-bands will correspond to the 6th harmonic of the electrical drive signal**.**

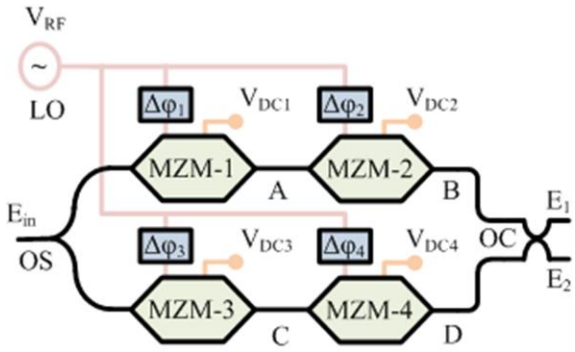

Fig. 5.2. Schematic diagram of the high-order sideband separation circuit using two series connected Mach-Zehnder modulators in parallel.

When a MZM is biased at its minimum transmission point, i.e. ($v_{DC} = v_\pi/2$), its amplitude transmission function can be written as:

$$h = \sin(\pi v/v_\pi) \tag{5.20}$$

When a two-stage cascade of MZMs is biased at MATP (according to the Fig 5.2, when($v_{DC1} = v_{DC2} = v_{DC3} = v_{DC4} = v_\pi/2$), the amplitude transmission functions of the two arms (MZM-1& MZM-2; MZM-3 & MZM-4) are:

$$h_{12} = \sin(\pi v_1/v_\pi)\sin(\pi v_2/v_\pi) \tag{5.21}$$

$$h_{34} = \sin(\pi v_3/v_\pi)\sin(\pi v_4/v_\pi) \tag{5.22}$$

Now the output of the whole circuit can be written:

$$\begin{bmatrix} E_1 \\ E_2 \end{bmatrix} = \frac{1}{2} H \begin{bmatrix} h_{12} & 0 \\ 0 & h_{34} \end{bmatrix} \begin{bmatrix} 1 \\ 1 \end{bmatrix} [E_{in}] \tag{5.23}$$

Developing Eq. (5.23) in the ideal case, the output is given by:

$$E_1 = \frac{1}{2}(h_{12} - ih_{34})E_{in} = -iE_2^* \tag{5.24}$$

$$E_2 = \frac{1}{2}(-ih_{12} + h_{34})E_{in} = -iE_1^* \tag{5.25}$$

With the aid of trigonometric identities, Eq. (5.21) & (5.22) can be re-expressed as:

$$h_{12} = \frac{1}{2}[\cos\{\pi(v_1 - v_2)/v_\pi\} - \cos\{\pi(v_1 + v_2)/v_\pi\}] \quad (5.26)$$

$$h_{34} = \frac{1}{2}[\cos\{\pi(v_3 - v_4)/v_\pi\} - \cos\{\pi(v_3 + v_4)/v_\pi\}] \quad (5.27)$$

Let the RF drive be given by $v_P = v_{RF}\cos(\omega_{RF}t + \Delta\varphi_P)$, where v_{RF} is the peak RF amplitude, ω_{RF} is the RF angular frequency, t is time and $\Delta\varphi_P$ is the phase of the RF drive to the MZM-. Setting the RF phase shifts to $\Delta\varphi_1 = 0$, $\Delta\varphi_2 = \pi/2$, $\Delta\varphi_3 = \pi/4$, and $\Delta\varphi_4 = 3\pi/4$ then:

$$v_1 - v_2 = v_{RF}[\cos(\omega_{RF}t) - \cos(\omega_{RF}t + \pi/2)] = \sqrt{2}v_{RF}\cos(\omega_{RF}t - \pi/4) \quad (5.28)$$

$$v_1 + v_2 = v_{RF}[\cos(\omega_{RF}t) + \cos(\omega_{RF}t + \pi/2)] = \sqrt{2}v_{RF}\cos(\omega_{RF}t + \pi/4) \quad (5.29)$$

$$v_3 - v_4 = v_{RF}[\cos(\omega_{RF}t + \pi/4) + \cos(\omega_{RF}t + 3\pi/4)] = \sqrt{2}v_{RF}\cos(\omega_{RF}t) \quad (5.30)$$

$$v_3 + v_4 = v_{RF}[\cos(\omega_{RF}t + \pi/4) + \cos(\omega_{RF}t + 3\pi/4)] = \sqrt{2}v_{RF}\cos(\omega_{RF}t + \pi/2) \quad (5.31)$$

and hence:

$$h_{12} = \frac{1}{2}[\cos\{m\cos(\omega_{RF}t - \pi/4)\} - \cos\{m\cos(\omega_{RF}t + \pi/4)\}] \quad (5.32)$$

$$h_{34} = \frac{1}{2}[\cos\{m\cos(\omega_{RF}t)\} - \cos\{m\cos(\omega_{RF}t + \pi/2)\}] \quad (5.33)$$

where:

$$m = \sqrt{2}\pi v_{RF}/v_\pi \quad (5.34)$$

is the modulation index.

The Jacobi-Anger expansion gives:

$$\cos(z\cos(\theta - \pi/4)) - \cos(z\cos(\theta + \pi/4)) = 4\sum_{l\ odd} J_{2l}(z)\cos(2l\theta - l\pi/2) = 4\sum_{l=2k+1}(-1)^k J_{2l}(z)\sin(2l\theta) \quad (5.35)$$

This implies:

$$h_{12} = 2\sum_{l=2k+1}(-1)^k J_{2l}(z)\sin(2l\theta) \quad (5.36)$$

Using Eq. (5.14), Eq. (5.33) can be written as:

$$h_{34} = 2\sum_{l=2k+1} J_{2l}(m)\cos(2l\omega_{RF}t) \quad (5.37)$$

Thus:

$$E_2 = \frac{1}{2}(-ih_{12} + h_{34})E_{in} = \sum_{l=2k+1} J_{2l}(m)[\cos(2l\omega_{RF}t) - i(-1)^k \sin(2l\theta)] =$$

$$\sum_{l=2k+1} J_{2l}(m) \exp(-i(-1)^k 2l\omega_{RF}t) \quad (5.38)$$

And hence:

Expanding the right-hand terms of Eq. (5.39) for the specified phase shifts $\Delta\varphi_P$ using the Jacobi-Anger expansion and eliminating the common terms, the output signal can be written as:

$$E_1 = -i[\, J_2(m) \exp(i2\omega_{RF}\mathrm{t}) + J_6(\mathrm{m})\exp(-i6\omega_{RF}\mathrm{t}) + J_{10}(m) \exp(i10\omega_{RF}\mathrm{t}) \ldots]E_{in} \quad (5.39)$$

$$E_2 = [\, J_2(m) \exp(-\mathrm{i}2\omega_{RF}\mathrm{t}) + J_6(\mathrm{m})\exp(\mathrm{i}6\omega_{RF}\mathrm{t}) + J_{10}(m) \exp(-\mathrm{i}10\omega_{RF}\mathrm{t}) \ldots]E_{in} \quad (5.40)$$

Hence, it is verified that both architectures generate the same sequence of orders Comparing Eq. (5.15) & (5.26) is can be seen that the required RF power for a two stage series-parallel architecture is 3 dB less than of the functionally equivalent single stage parallel structure. On the other hand, the single stage parallel circuit is more tolerant to the non-idealities encountered in practice such as power splitting imbalance of the optical coupler, phase imbalance and phase errors of the RF signals driving the modulators as discussed in chapter 4.

The use of the intrinsic phase relationship between ports of the 2× 2 multimode interference coupler (MMI), 1× 2 splitter and 2× 1combiner to define the operating point eliminates the need for large dc bias avoiding issues of drift., respectively can avoid the need for large static DC bias as discussed in chapter 2. Application of this design principle leads to the replacement of the DC-biased MZM mentioned in Fig 5.1 and Fig 5.2 by the dc bias-less MZM shown in Fig 5.3. Similarly the remaining optical couplers and optical splitters (Y-branch) may be replaced by 2× 2 MMI and symmetric 1× 2 MMI respectively. The circuit designed herein may be implemented using the $LiNbO_3$ integration platform, the most mature technology today to implement the MZM. However, its high switching voltage (typically $V_\pi = 5\ V$) makes it difficult to driving the modulator to maximise the amplitude of the 2nd harmonics or to suppress the 2nd harmonics to make use of the 6th harmonics. Moreover, the operating point of $LiNbO_3$ electro-optic modulator drifts when in the presence of large static DC bias which mandates complex stabilization circuitry [23, 27].

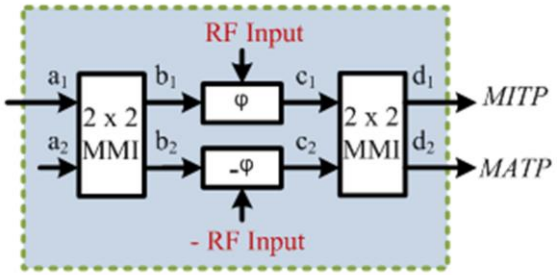

Fig. 5.3. Schematic of the MZM is formed by differentially driven phase modulators.

Silicon photonics is yet to offer a mature linear electro-optic modulator but recent developments in silicon or silicon hybrid (III-V or polymer) integration technology augurs well that ultimately these circuits will be able to benefit from denser integration offered by Silicon Photonics technology Noteworthy developments include the demonstration of Silicon-organic hybrid (SOH) IQ modulator for transmitting 16 QAM at 112 Gbit/s [50]; InAlGaAs-based electro-optic modulators with low drive voltage ($V_\pi = 0.77V$) and an exceeding bandwidth of 67 GHz [51]; athermal InP based twin IQ modulators having footprints of 1.2 mm × 13 mm for 56 Gb/s QPSK [52].

A schematic of the proposed down-link (optical to electrical channel) is shown in Fig 5.4 and is adopted from [7]. A continuous wave (CW) DFB laser is used to generate phase correlated harmonics (+2nd from upper and -2nd from lower) from the two output ports using the circuit described in the preceding. A pseudo random binary sequence (PRBS) is used as a digital baseband signal to externally modulate the phase of one of the harmonics (-2nd in this case) by using the DC bias-less I/Q modulator presented in chapter 1. As it requires no DC-bias, no drift is expected, which results in a robust design. A quadrature phase shift-keyed (QPSK) modulation format is implemented. The modulated harmonic (-2nd) and the un-modulated harmonic (+2) are combined and transported from the central office (CO) to the base station (BS) through a span of single mode optical fibre. Once the transmitted optical signal impinges in the photo-diode at the base station, a modulated RF carrier is generated with a carrier frequency of 4× f_{RF}. Where, f_{RF} is the applied RF local oscillator frequency at the central office. In this simulation f_{RF} is 10 GHz which results in a 40 GHz mm-wave RF carrier. Suppressing the 2nd order harmonics, a 12× f_{RF} RF carrier can be achieved, which would reduce the required RF frequency to 5 GHz. Before being radiated out by an antenna

to the end user, the modulated signal is passed through a RF amplifier, and a band-pass filter. The modulated mm-wave carrier is demodulated at the end user and the symbol error rate (SER) is measured. The wireless link was not implemented in the simulations but emulated by a given amount of loss and a noise source is used to model the noise floor of the receiver antenna.

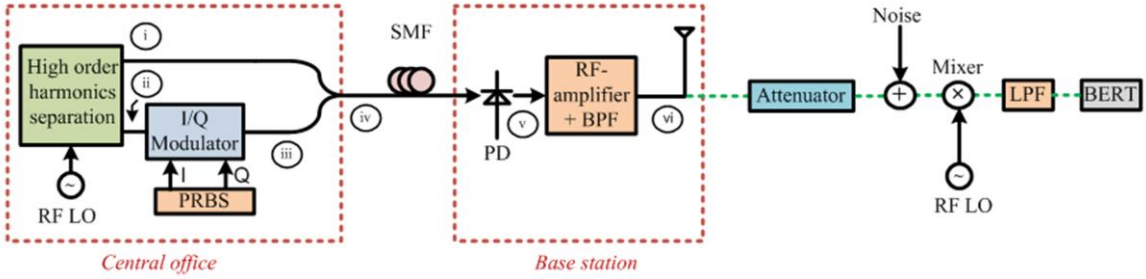

Fig. 5.4. Schematic diagram of the down-link**;** PRBS, pseudo-random binary sequence; SMF, single mode fibre; PD, photodetector; BPF, band-pass filter; LPF, low pass filter; BERT, bit error rate tester.

5.3. Simulation results

The operation of the proposed circuit and the complete downlink was verified by computer simulations using the Virtual Photonics Inc. (VPI) software package. A continuous-wave DFB laser diode operating at a vacuum wavelength of 1550 nm with a line-width of 200 kHz and an emission power of 10 mW is used as the optical input. The design that uses MZMs as presented in Fig. 3 is used for this simulation. A peak RF voltage of $v_{RF} = 1.18$ V, with a RF drive frequency, f_{RF} =10 GHz is used. The half-wave voltage, v_π of the phase modulators is set to 1 V [22]. The phase of the applied signals to the eight phase modulators (from top to bottom) is set to 0 & π (MZM_1), $\pi/2$ & $3\pi/2$ (MZM_2), $\pi/4$ & $5\pi/4$ (MZM_3), and $3\pi/4$ & $7\pi/4$ (MZM_4). In the ideal case, the power split (50%); the phase relations among the output ports of all the MMIs; and the phase shifts applied to the RF drive; are exactly as specified by the design. The circuit then generates $+2f_{RF}$ (20 GHz) and $-2f_{RF}$ (-20 GHz) harmonics from the two output ports as shown in Fig. 5 (i) & (ii). The next strongest harmonics are the 6^{th} harmonics. A 10 Gbit/s QPSK signal is generated from pseudo random binary sequences (PRBS) of period $2^{15} - 1$. This electrical signal modulates

the $-2f_{RF}$ optical carrier using I/Q modulation. The novel I/Q modulator architecture reported in references [22, 23] is used to perform the modulation. The output spectrum of the modulator is shown in Fig. 5 (iii). The output of the modulator is then combined with the un-modulated optical carrier at $+2f_{RF}$ using a 2×1 MMI or Y-combiner. The output of the combiner is shown in Fig 5 (iv). The output of the modulator is then combined with the un-modulated optical carrier at $+2f_{RF}$ using a 2×1 MMI or Y-combiner. The output of the combiner is shown in Fig 5 (iv).

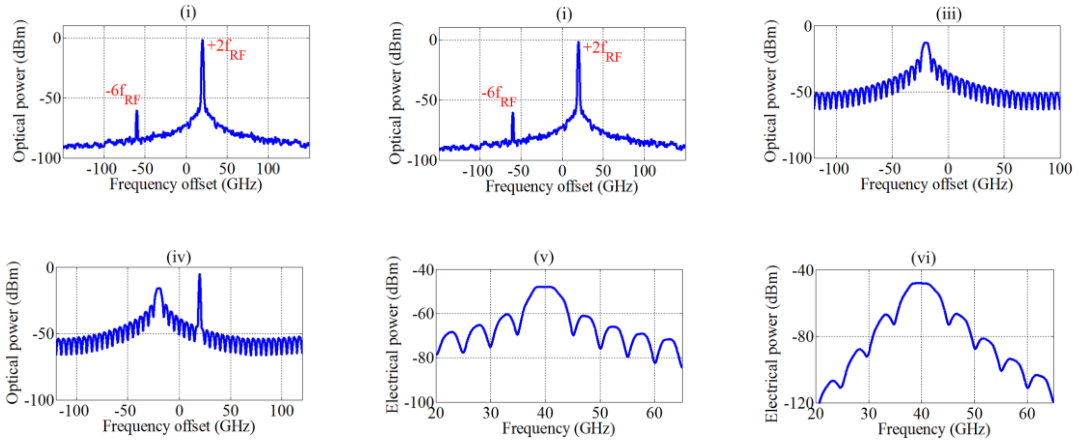

Fig. 5.5. Simulation results at the different stages of the proposed down-link architecture (Fig 5.4). A resolution bandwidth of 1 GHz is used in the both optical and electrical spectrum to record the data.

The combined output is then passed through a single mode fiber (SMF) to the remote base station and then detected by a square law photodiode with a 50-Ω load.. The frequency of the generated carrier (photonic approach) is determined by the relative frequency difference $[2f_{Rf} - (2f_{RF})] = 4f_{RF}$ of the strongest harmonics and is set to 40 GHz in this simulation. Hence the information signal (PRBS in this case) is imprinted on the 40 GHz carrier. The modulated carrier is then amplified and filtered through a band-pass filter having center frequency at 40 GHz with a bandwidth equal to the bit rate. Fig 5 (v) and (vi) show the power spectrum of the modulated signal before and after the band pass filter. The corresponding signal is then transmitted by antenna to provide the down-link of a wireless access system. In this simulation, the wireless link is emulated by using an attenuator with a given amount of loss and a Gaussian noise source is used to set the noise floor referred to the input of the receiver.

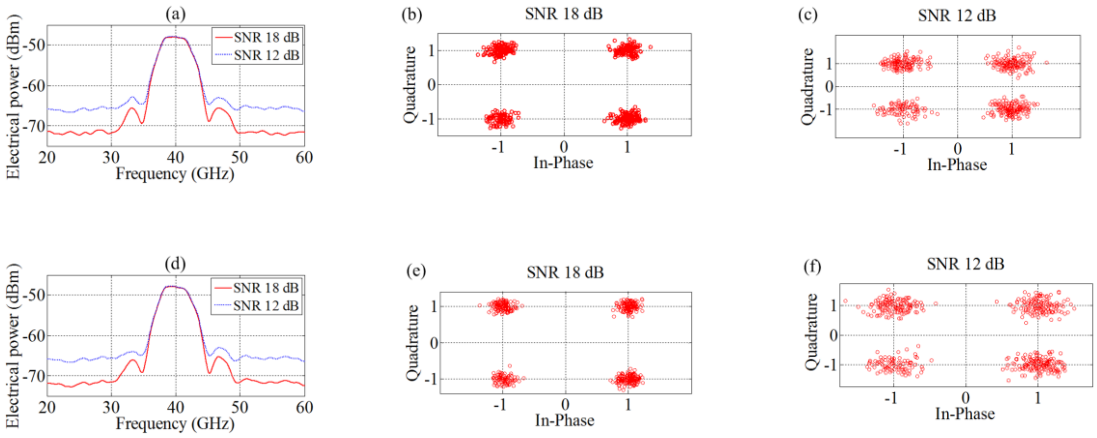

Fig. 5.6. (a) Electrical spectrum at different SNR for transmission without fibre (b) constellation diagram at 18 dB SNR with measured EVM of 10%; (c) constellation diagram at 12 dB SNR (EVM is 20%); (d) electrical spectrum at different SNR for 50 km transmission through fibre (e) constellation diagram at 18 dB SNR with measured EVM of 11% (f) constellation at 12 dB SNR with an EVM of 21%.

Fig. 5.6 (a) shows the received electrical signal spectrum at particular signal to noise ratio (SNR) when the optical signal impinges upon the photo-detector without transmission through fibre. Fig. 5.6(b) shows the corresponding constellation diagram of the received signal (In-phase channel and Quadrature-phase channel) once it is demodulated by a coherent receiver with a local oscillator having frequency equal to the transmitted carrier. The simulated error vector magnitude (EVM) is found to be 10% for a SNR of 18 dB. Fig 5.6(c) shows the constellation diagram when the SNR is 12 dB and the simulated EVM is 20% in this case. Fig. 5.6 (d) shows the received signal spectrum when the optical signal is transmitted via a 50 km span of standard single mode fibre (SMF) before it impinges on the photo-detector and generates the RF signal. The dispersion coefficient of the fibre span is set to $16 \times 10^{-6}\, s/m^2$ and the fibre attenuation coefficient is set to 0.2 dB/km. The self-phase modulation (SPM) effect is also considered in the simulation. There is no visual difference between the power spectra shown in Fig 5.6(a) & (d), but the constellation diagram presented in Fig 5.6(e) shows the impact of the fibre is a slight deterioration of signal quality. The calculated EVM is about 11 %, which is 1% greater than the case with no transmission via a fibre for same SNR. Fig 5.6 (f) shows the constellation diagram for SNR of 12 dB. Note that,

the input optical power was increased by 10 dB to compensate for the attenuation of the fibre, which ensures a fair comparison. An analysis of symbol error rate (SER) and EVM is presented to characterise the impact of the fibre on performance and a comparison is made with the performance of QPSK transmission over an AWGN channel which is named as "conventional" in the plot. The QPSK transmission over an AWGN channel is simulated using a QPSK transmitter and receiver for the same bitrate, i.e 10 Gbps and frequency, i.e 40 GHz as mentioned above.

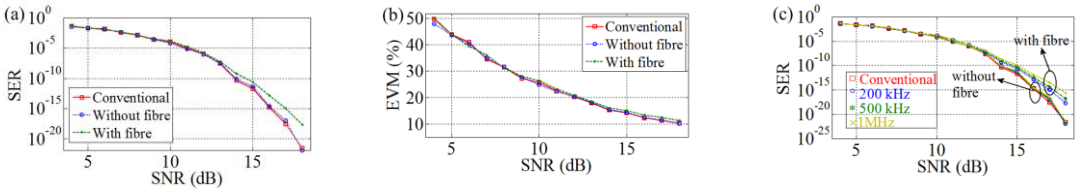

Fig. 5.7. Dependence of SER (a) and EVM (b) on SNR for 10 Gbit/s QPSK signals for transmission with and without fibre (c) dependence of SER on SNR for different line width of the laser.

Fig 5.7 (a) demonstrates the dependence of SER on SNR for different methods (conventional, with and without fibre) when the laser line width is set to 200 kHz. It shows that, all three curves are almost coincident up to a SNR of 13 dB and the SER at this point is approximately10^{-7}. As the SNR increases above 13 dB, the SER for fibre transmission slightly deviates from the ideal case. For example, the power penalty is 1 dB for a SER of 10^{-15}. Similarly, Fig 5.7 (b) shows the dependence of EVM on SNR for the same laser line width. It shows that the EVM is constant up to a SNR of 10 dB and above 10 dB, the EVM for transmission through fibre is 1% greater than the EVM for transmission without fibre, which is same as in the conventional case. As a measure of performance of the system (down-link), the dependence of SER on laser line width is further investigated. The SER is recorded for different values (200 kHz, 500 kHz, and 1000 kHz) of laser line-width and plotted in Fig 5.7 (c). Results shows, there is hardly any impact of laser line width on SER when the SNR is 13 dB and below.

A further investigation is carried to find out the reason for the deviation of SER from the ideal in Fig. 5.7 (a) when the SNR is above 13 dB. Fig. 5.8 (a) is a plot of SER versus SNR

for transmission through a fibre with zero dispersion and is coincident with the ideal curve for the full range of SNR up to 18 dB. This indicates that the inconsequential deviation from ideal performance is caused by the decorrelation of the phase noise contributed by the laser to both carriers due to the slight differential group delay resulting from chromatic dispersion and their frequency separation.

The optical power of the wanted harmonics (2^{nd}) can be maximized by adjusting the modulation index while retaining a modest suppression ratio with respect to the next strongest harmonics (6^{th}). Fig 5.8 (b) shows the dependence of the harmonic optical power (OP_2 & OP_6) and the corresponding suppression ratio (OP_2/OP_6) on modulation index (m) for an input optical power of 10 mW. The result shows that the 2^{nd} harmonic is at maximum when the modulation index is about 3, corresponding to a suppression ratio over 35 dB relative to the next strongest harmonics (6^{th}). For a $v_\pi = 1$V, m=3 leads to $v_{RF} = 0.95$ V, which corresponds to an RF power of 9.50 dBm for a load of 50-Ω. On the other hand, if the modulation index is adjusted to suppress the 2^{nd} harmonics (m~5.05 or ~8.30) , the strongest harmonic is the 6^{th}. This provides a frequency multiplication factor of 12, reducing the RF local oscillator frequency required by three times. For the same v_π as mentioned above, m=8.30 leads to $v_{RF} = 2.65$ V, which corresponds to an RF power of about 19 dBm well within the capability of an RF power amplifier (~25 dBm).

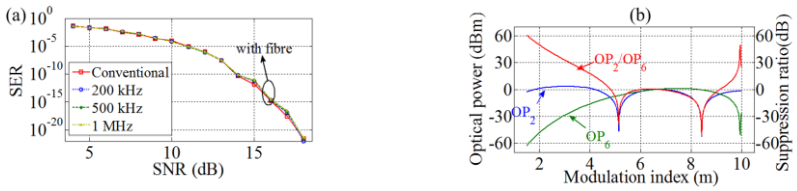

Fig. 5.8. (a) Dependence of SER on SNR for different laser line-width when the fibre dispersion is kept zero (b) dependence of harmonics optical power on modulation index and their suppression ratio; OP_2, optical power of 2^{nd} harmonics; OP_6, optical power of 6^{th} harmonics.

5.4. Conclusions

In summary, for the first time a novel photonic integrated circuit capable of separating single high order sidebands is presented. Two possible configurations are analyzed; a single-stage parallel MZM modulator configuration and a two-stage MZM with series-parallel architecture. Results show that the latter configuration requires 3 dB less RF power than the former configuration [19]. In addition, the SER as a function of SNR for both with and without transmission through a fibre span of 50 km has been evaluated and a comparison presented with the conventional QPSK system over an AWGN channel as a bench mark. The results show that, the proposed design has no deviation with the bench mark up to a SNR of 13 dB, at which point the SER is 10^{-7}. When the SER is very small (10^{-15}), the power penalty for transmission through fibre compared to the bench mark ranges from 1-1.5 dB depending on the laser line-width. It is found that the dispersion of the fibre is responsible for the deviation. Finally, the maturity of $LiNbO_3$ technology and continuous improvement in phase modulators based on silicon, III-V or hybrid technology ensures the implementation of the high order harmonics separation photonic integrated circuit is practical.

Chapter 6. Conclusions

6.1 Summary and Conclusions

The overall findings of the thesis can be summarized as:

1. A photonic integrated circuit capable of performing frequency up-conversion of an electrical domain signal to the optical domain and frequency octo-tupling of the RF signal has been proposed and verified by simulation. The proposed architecture can also be used as an I and Q modulator. Furthermore, the circuit requires no DC bias, as the static phase shifts are introduced using the intrinsic relative phase relations between the output and input ports of MMI couplers; hence, it is robust in design and energy-efficient. The SSB operation can be performed for a wide range of modulation indexes while the frequency octo-tupling is achieved by carefully adjusting the modulation index. Due to mature fabrication platforms for MMIs and significantly improving demonstration of phase modulators based on silicon, InGaAsP or hybrid technologies makes the implementation of the dual-function photonic integrated circuit practical.

2. Chapter 3 presents a theoretical approach based on N parallel phase modulators driven with progressive electrical $2\pi/N$ phase shift. A simulation verification of the theoretical prediction is presented for eight phase modulators which can be used for implementing frequency 8-tupling by carefully choosing the static optical phases. To overcome the requirement of static optical phase shift, a new design is proposed that uses the phase relation among the ports of 4×4 MMI. The proposed design overcomes the drawbacks of previously reported works as the scheme does not require any optical or electrical filters. Furthermore, the operation is not limited to carefully adjusted modulation indexes, and the drift originated from static DC bias is mitigated by making use of the intrinsic phase relations of multi-mode interference couplers. After analyzing the simulation results, the frequency 8-tupling and 24-tupling with an optical carrier and a harmonic distortion ratio of over 30 dB is achieved for inaccuracies on the 5% power imbalance of the input MMI and over 18 dB for 5° phase errors on the drive signals.

3. A novel photonic circuit architecture featuring a two-stage cascade MZM structure has been proposed for the first time for implementing frequency octo-tupling and quattuorviginti-tupling (24-tupling) and its operation analysed. The predictions of the theoretical analysis have been verified by computer simulations. The operation of the octo-tupler circuit is not restricted by any requirement to set the amplitude of the drive signal to a precise level. Moreover, in principal, the circuit requires no DC bias or optical filtering to suppress the unwanted harmonics. The analysis and simulations prove that the two-stage cascade MZM configuration is advantageous compared to the single-stage parallel MZM configuration with equivalent function, as it requires 3 dB less power in the RF drive for the same output when the applied RF signals reach the MZM with perfect phase relations. However, the single-stage parallel MZM configuration has a 4 dB advantage in Electrical SHSR compared to the two-stage serial-parallel MZM structure when imperfect scenarios such as phase errors of the RF signals are considered. Nevertheless, when the applied RF signal has no phase errors, over 30 dB harmonic suppression is obtained in both the optical and electrical domain when the extinction ratio of MZM is at least 25 dB and there is less than a 5% power imbalance between the ports of the input coupler.

4. Finally, for the first time a novel photonic integrated circuit for generating high-order single optical side-bands at the output port is presented. The operation principle of a single stage parallel MZM modulator configuration and two-stage MZM with series-parallel architecture is mathematically developed and simulation verification is provided. As an illustration of a prospective application it is shown how the circuit may be used to transport radio signals over fibre for wireless access, generating remotely an mm-wave carrier modulated by digital IQ data. A detailed calculation of Symbol error rate is presented for transmission through a fibre span of 50 km as a performance metric and a comparison is presented with the conventional QPSK system over an AWGN channel as a bench mark. The results show that, the proposed design has no deviation with the bench mark up to a SNR of 13 dB, at which point the SER is 10^{-7}. When the SER is very small (10^{-15}), the power penalty for transmission through fibre compared to the bench mark ranges from 1-1.5 dB depending on the laser line-width.

6.2 Discussion and Suggestions for Further Work

The simulation results are very encouraging to make these designs practical, but care must be taken for the following questions before practical implementation.

1. Silicon photonics has yet to offer a mature linear electro-optic modulator but recent developments in silicon or silicon hybrid (III-V or polymer) integration technology such as the demonstration of a silicon-organic hybrid (SOH) IQ modulator for transmitting 16 QAM at 112 Gbit/s [50]; InAlGaAs-based electro-optic modulators with low drive voltage ($v_\pi = 0.77v$) and an exceeding bandwidth of 67 GHz [51], and athermal InP-based twin IQ modulators having footprints of 1.2 mm × 13 mm for 56 Gb/s QPSK [52] augurs well for these circuits to ultimately be able to benefit from the denser integration offered by Silicon Photonics technology. Hence, the first priority is to find a mature linear electro-optic modulator.
2. The final priority is to address the challenge of applying RF drive signals to the phase modulators with a precise phase shift as per the design. Because the length of the waveguides connecting the drive signal to the phase modulators is found to be the critical design point among all the photonic integrated circuits proposed in this thesis as their performance degrades rapidly with phase error in the RF drive signal, it is important to know how the required phase shift of the RF drive signals for particular applications can be generated, which technology can be used for the phase shifter, and how the phase shifter can be integrated into the same chip.

References:

[1]ITU, "World Telecommunication Development Report: 1999, mobile cellular" https://www.itu.int/ITU-D/ict/publications/wtdr_99/material/wtdr99s.pdf (last accessed 21st May, 2015).

[2]http://mobiforge.com/research-analysis/global-mobile-statistics-2014-part-a-mobile-subscribers-handset-market-share-mobile-operators (last accessed 21st May, 2015).

[3]https://www.itu.int/osg/spu/ni/mobileovertakes/Resources/Mobileovertakes_Paper.pdf (last accessed 21st May, 2015).

[4]A. Ng'oma, "Radio over fibre technology for broadband wireless communication system" Ph.D. thesis, Faculty of Engineering, Eindhoven University of Technology, Denmark, June 28, 2005.

[5]http://en.wikipedia.org/wiki/Universal_Mobile_Telecommunications_System (Last accessed 21st May, 2015).

[6] http://en.wikipedia.org/wiki/LTE_Advanced (Last accessed 21st May, 2015).

[7]Trevor Hall, Ramon Maldonado-Basilio, Sawsan Abdul-Majid, Li Ran, Irene Antolín Pérez, Frédéric Lucarz, Jean-Louis de Bougrenet de La Tocnaye, Bruno Fracasso, Patrice Pajusco, Camilla Kärnfelt, Daniel Bourreau, Michel Ney, Rabiaa Guemri, Yves Josse, Hexin Liu, 'Radio-over-Fibre Access for Sustainable Digital Cities', Annals of Telecommunications, Springer, 2013.

[8] M. Izutsu, S. Shikama, T. Sueta, 'Integrated optical SSB modulator / frequency shifter', 'IEEE JQE, 17(11), 1981, pp. 2225-2227.

[9]M.-T. Zhou, A. B. Sharma, Z.-H. Shao, and M. Fujise, "Optical single-sideband modulation at 60 GHz using electro-absorption modulators," International Topical Meeting on Microwave Photonics, 121-124 (2005).

[10]D. Zibar, R. Sambaraju, A. Caballero Jambrina , R. Alemany, J. Herrera, I. Tafur Monroy, '16 Gb/s QPSK Wireless-over-Fibre Link in 75-110GHz Band Employing Optical Heterodyne Generation and Coherent Detection', ECOC 2010, 19-23 September 2010, Torino, Italy

[11]A. Caballero, D. Zibar, R. Sambaraju, J. Marti, I. T. Monroy, 'High-capacity 60 GHz and 75-110 GHz band links employing all-optical OFDM generation and digital coherent detection," Journal of Lightwave Technology, 30(1), 147-155, 2012.

[12]G. H. Smith, D. Novak, and Z. Ahmed, "Overcoming chromatic-dispersion effects in fiber-wireless systems incorporating external modulators," IEEE Trans. Microw. Theory Techn. 45(8), 1410-1415 (1997).

[13]G. H. Smith, D. Novak, and Z. Ahmed, "Technique for optical SSB generation to overcome dispersion penalties in fibre-radio systems," Electron. Lett. 33(1), 74-75 (1997).

[14]J. Yu, Z. Jia, L. Yi, Y. Su, G.-K. Chang, and T. Wang, "Optical millimeter-wave generation or up-conversion using external modulators," IEEE Photon. Technol. Lett. 18(1), 265-267 (2006).

[15]A. Wen, M. Li, L. Shang, and Y. Chen, "A novel optical SSB modulation scheme with interfering harmonics suppressed for ROF transmission link," Optics & Laser Technology 43, 1061–1064(2011).

[16]C. W. Chow, C. H. Wang, C. H. Yeh, and S. Chi, "Analysis of the carrier-suppressed single-sideband modulators used to mitigate Rayleigh backscattering in carrier-distributed PON" OPTICS EXPRESS 19(11), 10973 (2011).

[17]M. Bachmann, P. A. Besse, H. Melchior, 'General self-imaging properties in N×N multimode interference couplers including phase relations', Applied Optics, 33(18) pp. 3905-3911, 20 Jun. 1994.

[18]H. Nikkhah, Q. Zheng, I. Hassan, S. Abdul-Majid, T. J. Hall, 'The Free Space and Waveguide Talbot Effect: Phase Relations and Planar Light Circuit Applications', Photonics North 2012, Montreal, Canada, June 2012, Proc. SPIE 8412, 2012, art. 841217 (11 pages).

[19]Marcus Winter, Optical I-Q modulator, European Patent Application EP 2 141 833 A1, 2008.

[20]E. Vergol, F. Devaux, D. Tanguy, and E. Penard, "Integrated lightwave millimetric single side-band source: design and issues," IEEE J. Lightw. Technol. 16(7), 1276-1284 (1998).

[21]J.-G. Zhao, Z.-J. Liu, X.-L. Liu, T. Shang, and P. Yue, "Generation of radio signals using a novel Mach-Zehnder modulator with four arms," Opt. Commun. 282, 4353-4357 (2009).

[22]J.-G. Zhao, Z. J. Liu, X.-L. Liu, T. Shang, and P. Yue, "Optimisation of carrier-to-sideband ratio by triple-arm Mach-Zehnder modulators in radio-over-fibre links," IET Optoelectron. 4(5), 183-188 (2010).

[23]J. P. Salvestrini, L. Guilbert, M. Fontana, M. Abarkan, and S. Guille, "Analysis and control of the DC drift in LiNbO3-based Mach-Zehnder modulators," Journal of Lightwave Technology, 29(10), 1522-1534, (2011).

[24]R. Thapliya, S. Nakamura, and T. Kikuchi, "Investigation of drift in electro-optic polymer waveguides," Applied Physics Letters, 93(193309), (2008).

[25]S. M. Bilal, and G. Bosco, "Automatic bias control of Mach-Zehnder modulators for QPSK and QAM systems," Journal of Optics Technology, 81(7), 403-407, (2014).

[26]H. Kawakami, E. Yoshida, and Y. Miyamoto, "Auto bias control technique based on asymmetric bias dithering for optical QPSK modulation," Journal of Lightwave Technology, 30(7), 962-968, (2012).

[27]Y. Li, Y. Zhang, and Y. Huang, "Any bias point control technique for Mach-Zehnder modulator," IEEE Photonics Technology Letters, 25(24), 2412-2415, (2013).

[28]M. Sotoodeh, Y. Beaulieu, J. Harley, and D. L. McGhan, "Modulator bias and optical power control of complex E-field modulators," Journal of Lightwave Technology, 29(15), 2235-2248, (2011).

[29]J. J. O'Reilly, P. M. Lane, R. Heidemann, and R. Hofstetter, "Optical generation of very narrow linewidth millimeter wave signals," Electronics Letters, 28 (25), 2309-2311, (1992).

[30]G. Qi, J. Yao, J. Seregelyi, S. Paquet, and C. Bélisle "Generation and distribution of a wide-band continuously tunable millimeter-wave signal with an optical external modulation technique," IEEE Transactions on Microwave Theory and Techniques, 53(10), 3090-3097, (2005).

[31]J. Yu, Z. Jia, T. Wang, and G. K. Chang, "Centralized lightwave radio-over-fiber system with photonic frequency quadrupling for high-frequency millimeter-wave generation," IEEE Photonics Technology Letters, Vol. 19, No. 19, 1499-1501, (2007).

[32]C. T. Lin, P. T. Shih, J. Chen, W. Q. Xue, P. C. Peng, and S. Chi, "Optical millimeter-wave signal generation using frequency quadrupling technique and no optical filtering," IEEE Photonics Technology Letters, 20(12), 1027-1029,(2008).

[33]P. Shi, S. Yu, Z. Li, J. Song, J. Shen, Y. Qiao, and W. Gu, "A novel frequency sextupling scheme for optical mm-wave generation utilizing an integrated dual-parallel Mach-Zehnder modulator" Optics Communications 283, 3667-3672, (2010).

[34]S. Pan, and J. Yao, "Tunable sub-terahertz wave generation based on photonic frequency sextupling using a polarization modulator and a wavelength-fixed notch filter," IEEE Transactions on Microwave Theory and Techniques, Vol. 58, No. 7, 1967-1975,(2010).

[35]Y. Zhang and S. Pan, "Experimental demonstration of frequency-octupled millimeter-wave signal generation based on a Dual- Parallel Mach-Zehnder modulator," Microwave Workshop Series on Millimeter Wave Wireless Technology and Applications (IMWS), 1-4, (2012).

[36]J. Ma, X. Xin, J. Yu, C. Yu, K. Wang, H. Huang, and L. Rao, "Optical millimeter wave generated by octupling the frequency of the local oscillator," Journal of Optical Networking, 7(10), 837-845, (2008).

[37]R. Guemri, F. Lucarz and T. J. Hall, "Filter less millimeter-wave optical generation using optical phase modulators without DC bias," IEEE 10th Conference on Ph.D. Research in Microelectronics and Electronics (PRIME), Grenoble (2014).

[38]X. Yin, A. Wen, Y. Chen, and T. Wang, "Studies in an optical millimeter-wave generation scheme via two parallel dual-parallel Mach–Zehnder modulators" Journal of Modern Optics 58 (8),665-673 (2011).

[39]P.-T. Shih, J. Chen, C.-T. Lin, W.-J. Jiang, H.-S. Huang, P.-C. Peng, and S. Chi, "Optical millimeter-wave signal generation via frequency 12-tupling," Journal of Lightwave Technology, 28(1), 71-78, (2010).

[40]Z. Zhu, S. Zhao, Y. Li, X. Chu, X. Wang, and G. Zhao, " A radio-over-fiber system with Frequency 12-tupling optical millimeter-wave generation to overcome chromatic dispersion," Quantum Electronics Letters, 49(11), 919-922, (2013).

[41]Y. Chen, A. Wen, J. Guo, L. Shang, and Y. Wang, "A novel optical mm-wave generation scheme based on three parallel Mach–Zehnder modulators," Optics Communications 284, 1159–1169, (2011).

[42]J. Zhang, H. Chen, M. Chen, T. Wang, and S. Xie, “A photonic microwave frequency quadrupler using two cascaded intensity modulators with repetitious optical carrier suppression”, IEEE Photonics Technology Letters, 19(14), 1057-1059, (2007).

[43]H. Chi and J. Yao, “Frequency quadrupling and up conversion in a radio over fiber link,” Journal of Lightwave Technology, 26(15), 2706-2711, (2008).

[44]M. Mohamed, X. Zhang1, B. Hraimel, and K. Wu, “Frequency sixupler for millimeter-wave over fiber systems,” Optics Express, 16(14), 10141-10151, (2008).

[45]W. Li, and J.Yao, “Microwave generation based on optical domain microwave frequency octupling,” IEEE Photonics Technology Letters, 22(1), 24-26, (2010).

[46]W. Li, and J. Yao, “Investigation of photonically assisted microwave frequency multiplication based on external modulation”, IEEE Transactions on Microwave Theory and Techniques, 58(11), 3259-3268 (2010).

[47]Y. Gao, A. Wen, Q. Yu, N. Li, G. Lin, S. Xiang, and L. Shang, “Microwave generation with photonic frequency sextupling based on cascaded modulators”, IEEE Photonic Technology Letters, 26(12), 1199-1202 (2014).

[48]R. Maldonado-Basilio, M. Hasan, H. Nikkah, S. Abdul-Majid, R. Gumeri, F. Lucarz, J-L. de Bougrenet and T. J. Hall, “Electro-optic up-conversion mixer amenable to photonic integration,” Journal of Modern Optics, 2015 (Online).

[49]D. Marpaung C. Roeloffzen, R. Heideman, A. Leinse, S. Sales, and J. Capmanyet, “Integrated microwave photonics”, Laser Photonics Rev., 7(4), 506-538, (2013).

[50]D. Korn, R. Palmer, H. Yu, P. C. Schindler, L. Alloatti, M. Baier, R. Schmogrow, W. Bogaerts, S. K. Selvaraja, G. Lepage, M. Pantouvaki, J. M. D. Wouters, P. Verheyen, J. V. Campenhout, B. Chen, R. Baets, P. Absil, R. Dinu, C. Koos, W. Freude, and J. Leuthold, “Silicon-organic hybrid (SOH) IQ modulator using the linear electro-optic effect for transmitting 16 QAM at 112 Gbit/s,” Optics Express, 21(11), 13219-13227 (2013).

[51]S. Dogru, and N. Dagli, “0.77-V drive voltage electro-optic modulator with bandwidth exceeding 67 GHz,” Optics Letters, 39(20), 6074-6077, (2014).

[52]Y. Ogiso, Y. Nakanishi, S. Kanazawa, E. Yamada, H. Tanobe, M. Arai, Y. Shibata, and M. Kohtoku, “Planar n-SI-n heterostructure atermal InP (110) optical modulator,” Optics Express, 22(21), 25776-25781, (2014).

[53]M. J. R. Heck, J. F. Bauters, M. L. Davenport, J. K. Doylend, S. Jain, G. Kurczveil, S. Srinivasan, Y. Tang, and J. E. Bowers, “Hybrid silicon photonic integrated circuit technology,” IEEE J. Sel. Topics Quantum Electron. 19(4), 6100117 (2013).

[54]R. Halir, P. J. Bock, P. Cheben, A. Ortega-Monux, C. Alonso-Ramos, J. H. Schmid, J. Lapointe, D. Xu, J. G. Wanguemert-Perez, I Molina-Fernandez, and S. Janz, “Waveguide sub-wavelength structures: a review of principles and applications,” Laser Photonics Rev., 9(1),25-49 (2015).

[55]T. Kawanishi, T. Sakamoto, M. Tsuchiya, M. Izutsu, S. Mori, and K. Higuma, “70 dB extinction-ratio LiNbO3 optical intensity modulator for two-tone lightwave generation,” Proceedings of the Optical Fiber Communications Conference, OCW4, (2006).